Congenital mirror movements are associated with defective polymerization of RAD51

Oriane Trouillard, Pauline Dupaigne, Margaux Dunoyer, Mohamed Doulazmi, Morten Krogh Herlin, Solène Frismand, Audrey Riou, Véronique Legros, Guillaume Chevreux, Xavier Veaute, et al.

Congenital mirror movements are associated with defective polymerization of RAD51

Trouillard Oriane[1,2], Dupaigne Pauline[3], Dunoyer Margaux[4], Doulazmi Mohamed[5], Herlin Morten Krogh[6], Frismand Solène[7], Riou Audrey[8], Legros Véronique[9], Chevreux Guillaume[9], Veaute Xavier[10], Busso Didier[10], Fouquet Coralie[2], Saint-Martin Cécile[11], Méneret Aurélie[2,12], Trembleau Alain[2], Dusart Isabelle[2], Dubacq Caroline*[2] and Roze Emmanuel*[2,12]

(1) Sorbonne Université, INSERM, CNRS, Institut de Biologie Paris Seine, IBPS, Neuroscience Paris Seine, NPS, F-75005 Paris, France

(2) Sorbonne Université, Institut du Cerveau - Paris Brain Institute - ICM, Inserm, CNRS, AP-HP, Hôpital Pitié-Salpêtrière, Paris, France.

(3) Gustave Roussy, Genome Maintenance and Molecular Microscopy UMR9019 CNRS, Université Paris-Sud, Université Paris-Saclay, F-94805 Villejuif Cedex, France.

(4) AP-HP, Hôpital Pitié-Salpêtrière, Département de Neurologie, Paris, France.

(5) Sorbonne Université, INSERM, CNRS, Institut de Biologie Paris Seine, IBPS, Biological Adaptation and Ageing, B2A, F-75005 Paris, France.

(6) Department of Clinical Genetics, Aarhus University Hospital, Aarhus, Denmark.

(7) CHRU de Nancy, Service de Neurologie, Nancy, France.

(8) CHU Rennes, Service de génétique clinique &Service de neurologie, Rennes, France.

(9) Université Paris Cité, CNRS, Institut Jacques Monod, F-75013 Paris, France.

(10) Université Paris Cité, Université Paris-Saclay, Inserm, CEA, Stabilité Génétique Cellules Souches et Radiations, CIGEx/iRCM/IBFJ, F-92260 Fontenay-aux-Roses, France. (0000-0003-4868-247X)

(11) Sorbonne Université, AP-HP, Hôpital Pitié-Salpêtrière, Département de Génétique Médicale, Paris, France

(12) AP-HP, Hôpital Pitié-Salpêtrière, DMU Neuroscience 6, Paris, France; Sorbonne Université, Institut du Cerveau - Paris Brain Institute - ICM, Inserm, CNRS, AP-HP, Hôpital Pitié-Salpêtrière, Paris, France. (0000-0002-7623-1142)

*: co-last authors

Corresponding author:
Dubacq, Caroline
Sorbonne Université
BC16
9 quai Saint Bernard
75005 Paris
FRANCE
caroline.dubacq@sorbonne-universite.fr

Abstract

Background. Mirror movements are involuntary movements of one hand that mirror intentional movements of the other hand. Congenital mirror movements (CMM) is a rare genetic disorder with autosomal dominant inheritance, in which mirror movements are the main neurological manifestation. CMM is associated with an abnormal decussation of the corticospinal tract, a major motor tract for voluntary movements. RAD51 is known to play a key role in homologous recombination with a critical function in DNA repair. While RAD51 haploinsufficiency was first proposed to explain CMM, other mechanisms could be involved.

Methods. We performed Sanger sequencing of *RAD51* in five newly identified CMM families to identify new pathogenic variants. We further investigated the expression of wild-type and mutant RAD51 in the patients' lymphoblasts at mRNA and protein levels. We then characterized the functions of RAD51 altered by non-truncating variants using biochemical approaches.

Results. The level of wild-type RAD51 protein was lower in all the CMM patients' cells compared with their non-carrier relatives. The reduction was less pronounced in asymptomatic carriers. *In vitro*, mutant RAD51 proteins showed loss-of-function for polymerization, DNA binding, and strand exchange activity.

Conclusion. Our study demonstrates that *RAD51* haploinsufficiency, including loss-of-function of non-truncating variants, results in CMM. The incomplete penetrance likely results from post-transcriptional compensation. Changes in RAD51 levels and/or polymerization properties could influence guidance of the corticospinal axons during development. Our findings open up new perspectives to understand the role of RAD51 in neurodevelopment.

Key messages

WHAT IS ALREADY KNOWN ON THIS TOPIC

- To date, only four *RAD51* pathogenic variants have been associated with congenital mirror movements, a rare dominant neurodevelopmental condition with incomplete penetrance. The first reported variants were truncating, and the initial hypothesis was *RAD51* haploinsufficiency. The discovery of non-truncating pathogenic variants challenges this hypothesis.

WHAT THIS STUDY ADDS

- With the identification of four additional pathogenic variants, we provide new evidence for haploinsufficiency of *RAD51* in congenital mirror movements and suggest that compensation at the protein level could be a mechanism for incomplete penetrance. We found that variants alter RAD51 polymerization and DNA binding properties.

HOW THIS STUDY MIGHT AFFECT RESEARCH, PRACTICE OR POLICY

- Deciphering the molecular pathogenesis of *RAD51* variants in congenital mirror movements is a new step in understanding the various phenotypes related to *RAD51* pathogenic variants in humans. It also provides a new perspective for studying the role of RAD51 in neurodevelopment.

Main text

INTRODUCTION

Congenital mirror movements (CMM) [OMIM #614508] are characterized by involuntary movements of one hand that mimic and accompany voluntary movements performed by the opposite hand (1,2). CMM patients cannot perform pure unimanual movements and they have difficulties making bimanual movements which require independent activity of both hands (3). They often develop muscle and tendon pain in the upper limbs related to manual activities. The pathogenesis of CMM involves defects in the lateralization of motor control (4). CMM patients have corticospinal tract abnormalities at the level of the decussation, altered interhemispheric communication, and bilateral activation of primary motor areas during unimanual movements (5,6).

CMM is an autosomal dominant condition with incomplete penetrance. The established culprit genes are *DCC* (deleted in colorectal carcinoma [OMIM *120470]), *RAD51* (RAD51 recombinase [OMIM *179617]), and *NTN1* (Netrin 1 [OMIM *601614] (7–12). *DCC* encodes a receptor for Netrin 1 which promotes attraction and guidance of developing axons across the body's midline (13). RAD51 is well-known for its nuclear role in homologous recombination with a critical function in DNA repair (14). Its involvement in CMM was thus unexpected, and its possible role in the development of the motor system remains to be clarified.

Although pathogenic variants in *RAD51* represent the second genetic cause of CMM, little is known about the molecular link between these pathogenic variants and mirror movements (MMs). The actual consequence on transcription and protein expression has been poorly studied, as have the potential causes for incomplete penetrance. The first reported CMM-variants were truncating and the initial hypothesis was *RAD51* haploinsufficiency (Fig. 1A, upper panel) (9). Since then, non-truncating pathogenic variants have also been reported in

CMM patients (15,16). Interestingly, dominant negative *RAD51* non-truncating variants have been identified in three patients with atypical Fanconi anemia and in one patient with premature ovarian insufficiency, raising the possibility of distinct mechanisms in different RAD51 pathogenic contexts (17–20).

Here, we studied seven CMM-causing *RAD51* variants, truncating or non-truncating, including four new variants. We investigated RAD51 mRNA and protein levels in lymphocytes of both symptomatic and asymptomatic subjects from CMM families. The consequence of CMM-variants on RAD51 polymerization and DNA binding function was also tested.

PATIENTS AND METHODS

Patients.

We studied six index cases with typical CMM due to pathogenic variants in the *RAD51* gene, and their families. Each patient and available family members underwent a standardized neurologic assessment and DNA sampling. The severity of the MM was evaluated with the Woods and Teuber rating scale (21). Family history, MM location, and reported functional disability were noted (Table S1). Blood samples were obtained after informed and signed consent according to local ethics regulations. DNA was extracted using a standard protocol (11).

DNA sequence analysis and *in-silico* analysis.

Coding and flanking intronic regions of *RAD51* (GenBank accession no. NM_002875.5) were amplified from the patients' DNA samples, and Sanger sequenced as previously described (9,10). All the primers used in this study are listed in Table S2. No pathogenic variant was found in other CMM genes. Possible pathogenicity of missense variants was assessed *in-silico* with CADD (Combined Annotation Dependent Depletion (v1.6 with genome annotation GRCh38), PolyPhen-2 (Polymorphism Phenotyping v2) and SIFT (Sorting Intolerant From

Tolerant). Potential splicing effects of I292I and splice variants were predicted using Alamut Visual Plus software 1.4 (Sophia Genetics). All variants were classified according to the American College of Medical Genetics and Genomics guidelines (ACMG) (22).

Cell cultures and transfection.

The patients' lymphoblastoid cell lines (LCL) were established by Epstein-Barr virus transformation of the peripheral blood mononuclear cells and cultured using conventional methods (9).

Human embryonic kidney cells (HEK293) were transfected with indicated plasmids using Lipofectamine 2000 Reagent (Thermo Fisher Scientific). *RAD51* constructs were derived from the wild-type (WT) human *RAD51* cDNA (NCBI Reference Sequence: NM_002875 on GRCh38), or from the patients' gDNAs for *RAD51* hybrid minigenes, as detailed in the online supplementary data.

RNA splicing analysis and quantification.

Total RNAs were extracted using RNeasy Mini kit (Qiagen) and reverse transcribed with Superscript IV VILO kit, Thermo Fisher Scientific).

For splicing analysis, cDNAs were amplified by PCR separated on agarose gel, and then each band was individually purified by gel extraction and PCR clean-up kit (Macherey-Nagel) and Sanger sequenced. Splicing pattern of *RAD51* minigenes was analyzed as previously described (23). Briefly, the minigenes were transfected into HEK293 cells and the transcripts were analyzed by RT-PCR and agarose gel electrophoresis 24 hrs later.

Transcript quantification was performed by Allele-Specific Reverse Transcription-quantitative PCR (AS RT-qPCR) with GAPDH as the housekeeping gene and using the primers listed in Table S2.

Protein preparation and quantification.

Recombinant His-SUMO-RAD51 (24) was expressed in *E. coli* strain and purified as detailed in the online supplementary methods. Human RPA protein was purified as previously described (25).

Whole cell protein extracts were prepared, separated by SDS-PAGE, and analyzed by western blot following standard procedures (see online supplementary methods). All antibodies used for this study are listed in Table S3.

Mass spectrometry analysis of WT and mutant peptides from the patients' protein samples was performed as described in the online supplementary methods.

RAD51 co-immunoprecipitation.

48 hrs after transfection, whole cell extracts of HEK293 cells were prepared and 150 µg were incubated with 40 µL of Pierce Anti-Myc Magnetic Beads (Thermo Fisher Scientific). The beads were washed with IP buffer (500 mM Tris HCl [pH 7.5], 1% Tween-20, 3 M NaCl). Proteins were eluted at 95 °C with non-reducing Lane Marker Sample Buffer (Thermo Fisher Scientific). 5 µg of whole cell extracts (Input) and 25% of the immunoprecipitated (IP) fraction were analyzed by western blot.

RAD51 filament assembly and D-loop assay.

15 µM in nucleotides of DNA (NEB) were incubated with 2.5 or 5 µM RAD51 (1 protein per 6 or 3 nt, respectively) in reaction buffer (10 mM Tris-HCl [pH 7.5], 50 mM NaCl, 2 mM $MgCl_2$, 2 mM $CaCl_2$, 1.5 mM ATP, 1 mM DTT) 15 min at 37°C. For single-stranded DNA, 0.15 µM RPA (1 protein per 100 nt) were also added 3 min after RAD51. The reaction was quickly diluted 120 fold in reaction buffer without ATP and DTT, and 5 µL were deposited on

a 600-mesh copper grid previously covered with a thin carbon film and pre-activated by glow-discharge in the presence of amylamine (Sigma-Aldrich) (26,27). The grids were rinsed and positively stained with aqueous 2% (w/v) uranyl acetate, dried and observed in the annular dark-field mode in zero-loss filtered imaging using a Zeiss 902 transmission electron microscope. Images were captured at a magnification of 85,000x with a Veleta CCD camera and analyzed with iTEM software (Olympus Soft Imaging Solution).

6 μM in nucleotides of a 400-nt long Cy5-labeled single-stranded DNA substrate were incubated with 2 μM RAD51 (1 protein per 3 nt) in reaction buffer 15 min at 37°C. 5 μL of the reaction was crosslinked 5 min at RT in 0.01% glutaraldehyde, then separated on agarose gel. 10 μL of the reaction was added to 25 nmol in molecules of homologous pUC19 plasmid dsDNA donor. After 20 min at 37°C, the reaction was stopped and deproteinized using 1% SDS, 12.5 mM EDTA and 0.5 mg/mL Proteinase K during 30 min at 37°C, then separated on agarose gel. The DNA displacement loop (D-loop) yield of three independent experiments was quantified using Image J software (NIH).

Statistical analysis.

Normality in variable distributions and homogeneity of variances across groups were assessed with the Shapiro-Wilk and Levene's tests, respectively. Variables were analyzed using one or two-way ANOVA followed by Tukey's or Dunnet's *post hoc* test for multiple comparisons. The statistical tests are described in the legend of each figure.

RESULTS

Novel *RAD51* pathogenic variants result in CMM.

We further analyzed the consequences of the *RAD51* nonsense variant, (c.760C>T, p.R254*) found in the previously reported Family A (9), focusing on three individuals with

various status: non-mutated (III.1, nA +/+), asymptomatic carrier (II.3, nA m/+), and affected (III.10, A m/+) (Fig. 1B, S1A). We also analyzed another CMM family, of Norwegian origin, harboring the same truncating variant (11). In addition, we identified five heterozygous variants that could be the cause of CMM in nine affected individuals from five newly identified CMM families (Families B to F; Fig. 1B), and two asymptomatic carriers (I.2 in Family B and I.1 in C), in line with the known incomplete penetrance in *RAD51*-CMM (9). The characteristics of the patients from the six families are summarized in Table S1. All affected individuals had typical MMs, and five of them reported difficulties in fine bimanual activities. No other neurological or non-neurological phenotype cosegregated with the *RAD51* variants.

In the index case of Family B, we found a variant in the canonic donor site of intron 8, (c.774+1G>C, p.?), transmitted by his asymptomatic mother (Fig. 1B, S1A). This variant was absent from the genome aggregation database (gnomAD) and was classified as pathogenic according to the ACMG guidelines (Table 1). *In-silico* analysis predicted exon 8 skipping, which was confirmed by cDNA analysis (Fig. 1C). An *in vitro* splicing assay confirmed that the c.774+1G>C variant did induce exon 8 skipping (Fig. 1D). Exon 8 skipping resulted in a frameshift and premature stop codon (PTC) (r.645_774del, p.R251Sfs*4). The resulting mutant mRNA is expected to be degraded by nonsense-mediated mRNA decay (NMD), as observed in Family A (9).

Family	A[c]	B	C	D	E	F
Geographic origin	French	Danish	French	French	French	French
Variant: genomic description[a]	g.40729620C>T	g.40729635G>C	g.40729954C>T	g.40731112_40731113del	g.40706212_40706217del	g.40729609G>A[d]
transcript description[a]	c.760C>T	c.774+1G>C	c.876C>T	c.954_955del	c.261_266del	c.749G>A[d]
Protein change[a]	p.(R254*)	p.(R215Sfs*4)	p.(I292=)	p.(C319Sfs*3)	p.(A89_T90del)	p.(R250Q)[d]
Predicted consequences	Nonsense, expect NMD	Frameshift, expect NMD	Synonymous	Frameshift, last exon, escape NMD	In-frame deletion	Missense
***In-silico* predictions: SIFT**	n.a.	n.a.	n.a.	n.a	n.a.	Deleterious
PolyPhen-2	n.a.	n.a.	n.a.	n.a.	n.a.	Possibly damaging
CADD	40	34	8.316	33	18	32
Allele frequency[b]	$7.423.10^{-6}$	0	0	0	0	0
ACMG Classification	Pathogenic (PVS1, PM2, PP1, PP4)	Pathogenic (PVS1, PM2, PP4)	VUS (PM2, PP4)	Likely pathogenic (PVS1_strong, PM2, PP1, PP4)	Likely pathogenic (PM2, PM4, PP1, PP4)	Likely pathogenic (PM2, PP1, PP3, PP4, PP5)

Table 1. Characteristics of patients with *RAD51* pathogenic variants.

NMD, nonsense-mediated decay; n.a., not applicable; SIFT, Sorting Intolerant From Tolerant; PolyPhen-2, Polymorphism Phenotyping v2; CADD, Combined Annotation Dependent Depletion; ACMG, American College of Medical Genetics and Genomics. [a] HGVS nomenclature, based on GRCh38 (hg38), NM_002875.5 and NP_002866; [b] Allele frequency in gnomAD, Genome Aggregation Database v3.1.2; non-neuro; [c] Family already studied in (9); [d] Same variant as in (16).

In Family C, the (c.876C>T, p.I292=) synonymous variant was identified in a son with CMM, transmitted from his asymptomatic father (Fig. 1B, S1A). This variant was classified as a variant of uncertain significance (VUS) according to the ACMG guidelines (Table 1). However, it was absent in gnomAD. We thus performed an *in-silico* analysis: only the ESE Finder and EX-SKIP algorithms predicted a disruption of the splicing donor site in exon 9 with possible exon skipping. Study of cDNAs from the patient's lymphoblasts did indeed reveal the presence of a *RAD51* transcript lacking exon 9 (Fig. 1C). An *in vitro* splicing assay confirmed that the c.876C>T synonymous variant did induce exon 9 skipping but in a very limited manner, with the full-length transcript remaining the major transcript (Fig. 1D). Exon 9 skipping resulted in a frameshift and a PTC occurring in the last exon of *RAD51*, (r.775_896del, p.F259Ifs*23), suggesting that the resultant mRNA may escape NMD.

In two affected subjects (mother and daughter) of Family D, we found a truncating variant corresponding to a deletion of two nucleotides, resulting in a frameshift and PTC in the last exon of *RAD51*, (c.954_955del, p.C319Sfs*3) (Fig. 1B, S1A). It was absent in gnomAD and was classified as likely pathogenic according to the ACMG guidelines (Table 1). The variant mRNA may escape NMD as in Family C.

In three affected subjects (two children and their mother) of Family E, we identified an in-frame deletion leading to the loss of two amino acids, (c.261_266del, p.A89_T90del) (Fig. 1B, S1A). This new variant deleted two highly conserved amino acids (Fig. S1B), was absent in gnomAD, and was classified as likely pathogenic according to the ACMG guidelines (Table 1).

In two affected subjects (mother and daughter) of Family F, we found a missense *RAD51* variant, (c.749G>A, p.R250Q) (Fig. 1B, S1A). The same missense variant has been reported in a CMM family from North America (16).

In summary, NMD of the mutant mRNAs was probably present in Families A and B, whereas mutant proteins could exist in Families C-F.

Pathogenic variants induce CMM through *RAD51* haploinsufficiency.

We challenged the hypothesis of *RAD51* haploinsufficiency inducing CMM. We investigated whether the *RAD51* variants impact WT RAD51 levels and then we assessed the levels of mutant RAD51 (when present). To this purpose, we studied RAD51 expression in the lymphoblasts of the CMM patients by performing AS RT-qPCR, RT-PCR after emetin treatment, ddPCR, (see Supplementary experimental procedures in the online supplementary data) to specifically quantify WT and mutant *RAD51* mRNAs (Fig. 2, S2, S3, S4), and western blots to quantify proteins (Fig. 3).

For all the CMM families, WT *RAD51* mRNA levels were 44-78% lower in mutated individuals as compared with their non-mutated relatives (Fig. 2). The levels of WT *RAD51* mRNA were similar in the three asymptomatic carriers and their affected relatives (Fig. 2, S2). In Families A-D, the WT and mutated (if present) proteins were expected to be easily distinguished in western blot. Quantification of WT RAD51 proteins for these four families demonstrated a significant decrease of 33-51% in affected individuals as compared with non-mutated relatives (Fig. 3A). WT RAD51 protein levels were only 14-26% lower in asymptomatic carriers, two of them being significantly different from their affected relatives (Fig. 3A). For Families E and F, WT and mutant proteins were not distinguishable using western blot analysis. The levels of total RAD51 proteins (WT + mutant) were significantly lower only for one of the affected individuals (II.1 in Family E) as compared with non-mutated relatives (Fig. 3A). For Family E, mass spectrometry analysis of the characteristic peptides of WT and mutant RAD51 proteins found that the proportion of WT protein was 61 to 73% of total RAD51 proteins in affected subjects (Fig. 3B). The combination of the WT/total ratio estimated by mass

spectrometry and the total RAD51 protein levels measured by western blot estimated a 46-58% reduction in the WT protein in affected individuals of this family (Fig. S5). In Family F, although the characteristic peptides of the recombinant WT and mutant proteins were detected by mass spectrometry, the peptides could not be detected in the patients' cells.

Mutant mRNAs were detected at nearly undetectable levels in Families A and B (Fig. S2, S3). The increase in the mutant mRNA levels after emetin treatment (in (9) for A and Fig. S4 for B) confirmed the degradation of the mutant mRNAs by NMD in these families. In Family C, the mutant I292I mRNA was almost undetectable (Fig. S2, S3). The presence of the exon 9 skipping mRNA was detected at similar levels in the affected individual and the asymptomatic carrier, and was also detected in the non-mutated relative (Fig. S2). In Family D, the mutant mRNA was detected in the affected individual (Fig. S2, S3). The exon 9 skipping or mutant mRNA levels in Families C and D were unchanged after emetin treatment (Fig. S4) confirming that these mRNAs escaped NMD. For Families E and F (non-truncating variants), mutant mRNAs were detected at low levels (Fig. S2, S3).

In Families A-C, no mutant proteins were detected (Fig. 3A). Very low levels of proteins at the expected size of the exon 9 skipping isoform of RAD51 were present in the three members of Family C as well as in the non-mutated relative of other families (Fig. S6). Altogether, this exon 9 skipping isoform of RAD51 did not appear to be a specific product from the I292I allele, in line with the physiologic expression of this isoform (28). In Family D, the mutant protein was detected in the affected individual (Fig. 3A). For Family E, the mutant protein was detected in the patients' cells by mass spectrometry, contributing 27 to 39% of total RAD51 proteins in affected subjects (Fig. 3B).

To summarize, except for Family F where information was not available, WT RAD51 protein levels were lower in the lymphoblasts of all affected individuals in RAD51-CMM families compared with the non-mutated relatives. These pathogenic RAD51 levels tended to be lower

than those observed in asymptomatic carriers (Fig. S5). As predicted, NMD of the mutant mRNAs was confirmed in Families A and B, and mutant proteins were not detectable in these two families, or in Family C. In Families D and E, the mutant proteins were detected and contributed to more elevated levels of total RAD51 proteins (Fig. S5). In Family F, the WT and mutant proteins could not be distinguished and the high total RAD51 levels might be a result of pathogenic levels of WT RAD51 complemented by the mutant protein. Altogether, these results imply that the unknown neurodevelopmental function of RAD51 revealed by CMM is impaired in the mutated proteins of Families D-F (respectively p.C319Sfs*3; p. A89_T90del and p.R250Q).

Pathogenic variants alter polymerization of RAD51.

The three-dimensional structure of the filament formed by RAD51 polymerization indicated that the affected residues of CMM-mutated RAD51 proteins (A89, T134 (15), R250 and C319) were located at the interface of adjacent RAD51 protomers (Fig. 4A). The A89 residue was in the main RAD51-RAD51 interaction motif (29). The T134 and the C319 residues participated in ATP binding in the Walker A domain and the facing ATP cap (30), respectively, the two domains forming together a secondary RAD51-RAD51 interaction motif. The R250 residue was also involved in a secondary interaction motif, capping the end of an alpha helix in the adjacent protomer. Thus, these four *RAD51* pathogenic variants might theoretically influence RAD51-RAD51 interaction.

We therefore tested the ability of mutant proteins to interact with WT protein by co-immunoprecipitation. The C319Sfs*3 mutant protein is destabilized when expressed in heterologous systems and, therefore, could not be included in this part of the study (Fig. S7). An experimental variant altering one of the CMM mutated residues and studied in the literature, A89E, was included as a positive control of altered RAD51-RAD51 interaction (29). All mutant

RAD51 proteins tested showed a reduced relative co-immunoprecipitation efficiency compared with the WT RAD51 protein (Fig. 4B-C).

As the RAD51-RAD51 interaction is essential for RAD51 polymerization, we then tested this function *in vitro*. Whereas the WT RAD51 assembled in a long, continuous and homogenous nucleofilament on double-stranded DNA (dsDNA) or single-stranded DNA (ssDNA) (Fig. 5Aa-b, 5Ba-b), the three CMM-mutant RAD51 proteins failed to form a proper nucleofilament on ds- or ssDNA: rare fixation to DNA and no filament formation for A89_T90del (Fig. 5Ac, 5Bc), formation of discontinuous and irregular filaments for T134N and R250Q (Fig. 5Ad-e, 5Bd-e), with large aggregates for T134N. Electrophoretic mobility shift assays (EMSA) confirmed that the A89_T90del mutant protein failed to form stable complexes with ssDNA, whereas the T134N mutant protein could interact with DNA but was highly prone to aggregation, and the R250Q mutant protein formed less stable complexes with ssDNA than the WT protein (Fig. 5D). Furthermore, CMM-mutant RAD51 also lacked the capacity to form a D-loop (Fig. 5E-G), a homologous recombination intermediate DNA structure which is dependent on RAD51 activity (see WT on Fig. 5F-G). An equimolar mix of the WT and each of the mutant proteins did not noticeably change the aspect of the filament formed on ssDNA (Fig. 5C), the ssDNA binding (Fig. 5D), or the D-loop activity (Fig. 5F-G) of the same sub-saturating quantities of the WT protein only. Overall, the CMM-mutated RAD51 proteins included in this biochemical study showed loss-of-function in terms of RAD51-RAD51 interactions, nucleofilament formation, DNA binding and/or D-loop activity, but did not significantly alter the properties of the WT protein in an equimolar mix.

DISCUSSION

We describe here four new pathogenic variants of *RAD51* in CMM families, in addition to the four previously reported variants. We provide evidence supporting that *RAD51*

haploinsufficiency is the key molecular mechanism causing CMM. We propose that incomplete penetrance might be the result of a compensation at the protein level. When present, CMM-causing mutant RAD51 proteins result in abnormal polymerization. We thus speculate that a change in RAD51 levels and/or polymerization properties could influence axon guidance of the corticospinal tract during development of the motor system.

In a previous study, we identified two truncating variants causing CMM: (p.R254*) and (p.P286Tfs*37) (Fig. 1A, upper panel) (9). For the (p.R254*) nonsense variant, we demonstrated a downregulation of total *RAD51* mRNA by NMD resulting in the absence of mutant protein. This raised the possibility of *RAD51* haploinsufficiency in CMM (9,11). Here, we identified four new variants, namely two truncating variants (p.C319Sfs*3 and p.R215Sfs*4), a synonymous variant (p.I292=), and an in-frame deletion (p.A89_T90del) (Fig. 1A, lower panel). A total of eight variants, including three non-truncating (p.A89_T90del; p.T134N (15) and p.R250Q (16)), have thus been associated with CMM so far (Fig. 1A). No functional study has been performed on the non-truncating variants, except for the overexpression of the (p.R250Q) variant in primary cultures of mouse cortical neurons suggesting a loss-of-function of the mutant protein (31). The possible presence of the mutant RAD51 proteins and the functional consequences in patients' cells remain a matter of debate.

We studied the expression of WT-RAD51 for the four new CMM-related variants and two previously reported pathogenic variants. We found lower levels of WT-RAD51 in all affected CMM patients compared with non-mutated subjects at both mRNA and protein levels (when available). Moreover, the asymptomatic carriers had intermediate WT-RAD51 protein levels, lower than those of their non-mutated relatives but higher than affected individuals of the same family (Fig. S5). We further demonstrated either absence of the mutant proteins in

three families or loss-of-function of the mutant proteins in three other families. This formally demonstrates that *RAD51* haploinsufficiency causes CMM.

The decrease of RAD51 expression associated with the synonymous c.876C>T (p.I292I) variant of Family C was puzzling. We excluded a role of alternative splicing and we hypothesize that this synonymous codon could alter mRNA regulatory sequences (32).

The three asymptomatic carriers had WT-*RAD51* mRNA levels, similar to that of affected individuals, but intermediate protein expression levels. Therefore, post-transcriptional compensation is likely to account for incomplete penetrance by maintaining the WT-RAD51 protein level above a critical threshold. This compensation mechanism in *RAD51*-CMM families differs from the transcriptional compensation mechanism observed in a *DCC*-CMM family, in which the WT *DCC* mRNA levels of asymptomatic carriers is higher than that of non-mutated individuals (33).

In the nucleus, RAD51 polymerizes to form a nucleofilament with single-stranded DNA through the assembly of several RAD51 monomers (34). The four residues affected by the non-truncating CMM-variants (A89, T134, R250 and C319) are located at the interface between adjacent RAD51 protomers and are probably involved in RAD51-RAD51 interactions. We found an impaired interaction between the A89_T90del, T134N, and R250Q RAD51 mutant proteins and WT-RAD51, as previously shown for the experimental A89E variant (29). In addition, all three variants prevented the formation of regular nucleofilaments associated with an inability to interact with DNA and to form D-loops. Of note, in experimental conditions with sub-saturating levels of WT protein, addition of equimolar quantities of mutant RAD51 proteins did not interfere with the WT protein DNA binding, filament assembly, or D-loop activity. This argues against a dominant-negative effect of the mutant protein, in contrast to what has been described in variants related to atypical Fanconi anemia or premature ovarian insufficiency (17–

20). In CMM patients' cells, the WT-RAD51 protein is reduced (42-67% of WT-RAD51 levels in the intrafamilial controls) without any phenotypic evidence for alterations in its homologous recombination activity: in our CMM cohort, none of the patients with RAD51 pathogenic variants presented fertility problems, Fanconi anemia, or cancer. In line with this observation, the cellular levels of RAD51 are thought to exceed the cell's needs for homologous recombination (35). Our findings strongly support that both truncating and non-truncating *RAD51*-CMM variants result in a loss of function selectively associated with the CMM phenotype.

RAD51 is expressed in the cytoplasm of cortical neurons of neonate mice (9). This critically occurs within a spatiotemporal window corresponding to the midline crossing of the corticospinal tract (9). Impaired midline crossing of the corticospinal tract is a key and consistent feature in CMM patients (5,6). Together with the present findings, this suggests that a balanced RAD51 polymerization is important for its cytoplasmic role in the development of the corticospinal tract. This opens up a new framework to investigate the role of RAD51 in the cytoplasm.

Acknowledgments
The authors thank the patients and their families for their cooperation and support of this research.

Contributors
I.D., C.D. and E.R. designed the work. O.T., P.D., M.Du, M.K.H., S.F.K., A.R., V.L., G.C., X.V., D.B., C.F., C.S.-M. and A.M. acquired data. O.T., P.D., M.Du, M.Do analyzed data. O.T., P.D., M.Du, M.Do and A.T. interpreted data. O.T., C.D. and E.R. drafted the work. M.Du, M.Do, M.K.H., S.F.K., A.R., V.L., G.C., X.V., D.B., C.F., C.S.-M., A.M, A.T. and I.D. revised it for intellectual content. C.D. and E.R. contributed equally to this paper. All coauthors have approved the final version of the manuscript. Part of this work was carried out on the DNA & cells bank of the Paris Brain Institute and on the real-time PCR facility of IBPS. We gratefully acknowledge Ludmila Jornea and Sylvie Forlani for cellular immortalization. We thank the iGenSeq core facility of ICM for their advice on the ddPCR. Raphaël Guérois and Jessica Andreani contributed for helpful discussions and assistance.

Funding
This work was supported by the Fondation Desmarest, Merz-Pharma, Elivie, Orkyn, Djillali Mehri, CNRS, INSERM and Sorbonne Université. This work was also funded by grants from the Agence Nationale de la Recherche (ANR) (ANR-14-CE13-0004-01, ANR-18-CE16-0005-02), from the National Institute of Health NIDCD (R01-DC-017989, USA) and it was performed within the framework of LABEX LIFESENSES (ANR-10-LABX-65) supported by French state funds managed by the ANR within the Investissements d'Avenir program (ANR-11-IDEX-0004-02).

Competing interests
None

Data availability statement
Except for the raw data, no additional data are available. Raw data may be made available if it does not infringe patient's rights.

Patient consent
Written consent was obtained from all families.

Ethics approval
This study was approved by the ethics committee of the Hôpital de la Pitié-Salpêtrière and the Comité de Protection des Personnes (CPP), Ile-de-France 6, Paris

REFERENCES

1. Bonnet C, Roubertie A, Doummar D, et al. Developmental and benign movement disorders in childhood. *Mov Disord* 2010;25(10):1317–34.
2. Meneret A, Trouillard O, Brochard V, et al. Congenital mirror movements caused by a mutation in the DCC gene. *Dev Med Child Neurol* 2015;57(8):776–776.
3. Méneret A, Welniarz Q, Trouillard O, et al. Congenital mirror movements From piano player to opera singer. *Neurology* 2015;84(8):860–860.
4. Galléa C, Popa T, Billot S, et al. Congenital mirror movements: a clue to understanding bimanual motor control. *J Neurol* 2011;1;258(11):1911–9.
5. Gallea C, Popa T, Hubsch C, et al. RAD51 deficiency disrupts the corticospinal lateralization of motor control. *Brain* 2013;136(11):3333–46.
6. Welniarz Q, Dusart I, Gallea C, et al. One hand clapping: lateralization of motor control. *Front Neuroanat* 2015;9:75.
7. Srour M, Rivière JB, Pham JMT, et al. Mutations in DCC Cause Congenital Mirror Movements. *Science* 2010;328(5978):592–592.
8. Depienne C, Cincotta M, Billot S, et al. A novel DCC mutation and genetic heterogeneity in congenital mirror movements. *Neurology* 2011;76(3):260–4.
9. Depienne C, Bouteiller D, Méneret A, et al. RAD51 Haploinsufficiency Causes Congenital Mirror Movements in Humans. *Am J Hum Genet* 2012;90(2):301–7.
10. Meneret A, Depienne C, Riant F, et al. Congenital mirror movements: Mutational analysis of RAD51 and DCC in 26 cases. *Neurology* 2014;82(22):1999–2002.
11. Trouillard O, Koht J, Gerstner T, et al. Congenital Mirror Movements Due to RAD51: Cosegregation with a Nonsense Mutation in a Norwegian Pedigree and Review of the Literature. *Tremor Other Hyperkinet Mov (N Y)* 2016;3;6:424.
12. Méneret A, Franz EA, Trouillard O, et al. Mutations in the netrin-1 gene cause congenital mirror movements. *J Clin Invest* 2017;127(11):3923–36.
13. Finger JH, Bronson RT, Harris B, et al. The Netrin 1 Receptors Unc5h3 and Dcc Are Necessary at Multiple Choice Points for the Guidance of Corticospinal Tract Axons. *J Neurosci* 2002;22(23):10346–56.
14. Bonilla B, Hengel SR, Grundy MK, et al. RAD51 Gene Family Structure and Function. *Annu Rev Genet* 2020;54(1):25–46.
15. Demirayak P, Onat OE, Gevrekci AÖ, et al. Abnormal subcortical activity in congenital mirror movement disorder with RAD51 mutation. *Diagn Interv Radiol* 2018;24(6):392–401.
16. Franz EA, Chiaroni-Clarke R, Woodrow S, et al. Congenital mirror movements: Phenotypes associated with DCC and RAD51 mutations. *J Neurol Sci* 2015;351(1–2):140–5.
17. Wang AT, Kim T, Wagner JE, et al. A dominant mutation in human RAD51 reveals its function in DNA interstrand crosslink repair independent of homologous recombination. *Mol Cell* 2015;59(3):478–90.
18. Ameziane N, May P, Haitjema A, et al. A novel Fanconi anaemia subtype associated with a dominant-negative mutation in RAD51. *Nat Commun* 2015;6:8829.
19. Takenaka S, Kuroda Y, Ohta S, et al. A Japanese patient with RAD51-associated Fanconi anemia. *Am J Med Genet A* 2019;179(6):900–2.
20. Luo W, Guo T, Li G, et al. Variants in Homologous Recombination Genes EXO1 and RAD51 Related with Premature Ovarian Insufficiency. *J Clin Endocrinol Metab* 2020;105(10):e3566–74.
21. Woods BT, Teuber HL. Mirror movements after childhood hemiparesis. *Neurology* 1978;28(11):1152–7.
22. Richards S, Aziz N, Bale S, et al. Standards and Guidelines for the Interpretation of Sequence Variants: A Joint Consensus Recommendation of the American College of Medical Genetics and Genomics and the Association for Molecular Pathology. *Genet Med* 2015;17(5):405–24.
23. Soukarieh O, Gaildrat P, Hamieh M, et al. Exonic Splicing Mutations Are More Prevalent than Currently

Estimated and Can Be Predicted by Using In Silico Tools. *PLoS Genet* 2016;12(1):e1005756.
24. Martinez JS, von Nicolai C, Kim T, et al. BRCA2 regulates DMC1-mediated recombination through the BRC repeats. *Proc Natl Acad Sci U S A* 2016;113(13):3515–20.
25. Gomes XV, Henricksen LA, Wold MS. Proteolytic Mapping of Human Replication Protein A: Evidence for Multiple Structural Domains and a Conformational Change upon Interaction with Single-Stranded DNA. *Biochemistry* 1996;35(17):5586–95.
26. Veaute X, Jeusset J, Soustelle C, et al. The Srs2 helicase prevents recombination by disrupting Rad51 nucleoprotein filaments. *Nature* 2003;423(6937):309–12.
27. Dubochet J, Ducommun M, Zollinger M, et al. A new preparation method for dark-field electron microscopy of biomacromolecules. *J Ultrastruct Res* 1971;35(1):147–67.
28. Park JY, Yoo HW, Kim BR, et al. Identification of a novel human Rad51 variant that promotes DNA strand exchange. *Nucleic Acids Res* 2008;36(10):3226–34.
29. Pellegrini L, Yu DS, Lo T, et al. Insights into DNA recombination from the structure of a RAD51–BRCA2 complex. *Nature* 2002;420(6913):287–93.
30. Amunugama R, He Y, Willcox S, et al. RAD51 Protein ATP Cap Regulates Nucleoprotein Filament Stability. *J Biol Chem* 2012;287(12):8724–36.
31. Glendining KA, Markie D, Gardner RJM, et al. A novel role for the DNA repair gene Rad51 in Netrin-1 signalling. *Sci Rep*. 2017;7:39823.
32. Liu Y, Yang Q, Zhao F. Synonymous but not Silent: The Codon Usage Code for Gene Expression and Protein Folding. *Annu Rev Biochem* 2021;90:375–401.
33. Vosberg DE, Beaulé V, Torres-Berrío A, et al. Neural function in DCC mutation carriers with and without mirror movements. *Ann Neurol* 2019;85(3):433–42.
34. Carreira A, Hilario J, Amitani I, et al. The BRC Repeats of BRCA2 Modulate the DNA Binding Selectivity of RAD51. *Cell* 2009;136(6):1032–43.
35. Foertsch F, Kache T, Drube S, et al. Determination of the number of RAD51 molecules in different human cell lines. *Cell Cycle* 2019;18(24):3581–8.

Legend of the figures.

Figure 1. *RAD51* pathogenic variants in CMM families.
(**A**) Location of pathogenic variants on a schematic representation of the human RAD51 protein. Previously reported variants are in the upper panel. Novel pathogenic variants are in the lower panel. HhH, helix-hairpin-helix domain; AAA+, ATPase domain; circles, truncating variants; diamonds, non-truncating variants. (**B**) Pedigrees of the CMM families included in this study. m, mutated allele; +, wild-type allele. Black symbols represent individuals with CMM, symbols with an embedded black circle indicate asymptomatic carriers, white symbols indicate unaffected individuals. Note that all the genotyped relatives affected with CMM harbor the heterozygous *RAD51* pathogenic variant (m/+). Symbols with a diagonal line represent deceased individuals. Squares represent males, circles represent females and diamonds stand for additional family members who did not participate in this study. (**C**) cDNA sequences showing exon skipping in CMM index cases of two families. RNAs were extracted from the patient's lymphoblasts, and *RAD51* fragments spanning the presumed skipped exon from the mutant allele were amplified by RT-PCR. For each index case, the upper and lower panels show the Sanger sequencing of the wild-type and exon skipping alleles, respectively. (**D**) Representative result of *in vitro* analysis of the splicing pattern of minigenes containing these two exon-skipping variants. WT and mutant constructs in the pCAS2 vector were transfected into HEK293 cells and the minigenes' transcripts analyzed by RT-PCR and agarose gel electrophoresis (n=3). The RT-PCR products consist in exons A and B of the pCAS2 vector (grey boxes) +/- exon 8 (Family B) or 9 (Family C) of *RAD51* (white box). Empty: control construct with no *RAD51* exon; c.876+1G>A: control construct with a donor splice mutant resulting in *RAD51* exon 9 skipping.

Figure 2. Expression of WT *RAD51* mRNA in CMM families.
RNAs were extracted from patients' lymphoblasts and *RAD51* mRNA expression was quantified by allele specific RT-qPCR (n ≧ 3). For each family, the wild-type *RAD51* mRNA levels were normalized to a non-mutated relative. Data are represented as means ± S.E.M. Significance was calculated by 2-way ANOVA followed by Tukey's *post hoc* test (ns, non-significant; **P* < 0.05; ***P* < 0.01; ****P* < 0.001). A, affected; nA, non-affected; m, mutated allele; +, wild-type allele.

Figure 3. WT and mutant RAD51 proteins expression in CMM families.
(**A**) For each family, upper part shows a representative immunoblot performed on whole cell protein extracts from patients' lymphoblasts. Lower part shows the quantification of n ≧ 3 experiments: RAD51 protein levels were normalized to α-Tubulin, used as a loading control, and to the wild-type protein level of a non-mutated relative. Histograms in black correspond to full-length wild-type RAD51 protein, in white to mutant RAD51 protein, in grey to undistinguishable wild-type and mutant RAD51 proteins (total RAD51 protein). Data are represented as means ± S.E.M. Significance was calculated by 2-way ANOVA followed by Tukey's *post hoc* test (ns, non-significant; **P* < 0.05; ***P* < 0.01; ****P* < 0.001). A, affected; nA, non-affected; m, mutated allele; +, wild-type allele. (**B**) For one family with a non-truncating *RAD51* pathogenic variant (Family E), immunoprecipitation of RAD51 protein was performed on whole cell protein extracts from affected patients' lymphoblasts, followed by tandem mass spectrometry analysis. Both the wild-type and the A89_T90del mutant RAD51 proteins were identified by generating extracted ion chromatograms (XIC) of their characteristic peptides LVPMGFT(TA/)TEFHQR, which distinguish the wild type from mutant RAD51 protein. The relative expression ratio of the two isoforms was assessed by calculating the ratio of XIC peak areas. RT, retention time; AA, peak area.

Figure 4. Effect of *RAD51* pathogenic variants on RAD51-RAD51 interaction.
(**A**) The CMM-mutated residues are located at the interface between RAD51 protomers. Cartoon representation of the structure of human RAD51-ATP filament (PDB = 5NWL; each color corresponds to one protomer) showing in the insets the A89, T134, R250 residues as sticks, the C-terminal end of the protein starting from C319 in yellow. A89 is located at the interface between two RAD51 protomers. T134 is forming a hydrogen-bond with the second phosphate of the ATP. C319 is in the ATP cap (D316-P321). ATP is sandwiched between the ATP binding site and the ATP cap of the adjacent protomer. R250 faces the C-terminal end (containing D231) of an alpha-helix of the adjacent protomer. In the form where RAD51 binds ssDNA (PDB = 5H1B), R250 forms a salt-bridge with D231. (**B**) Representative immunoblots of RAD51 co-immunoprecipitations experiments. The upper panel (Input) shows whole cell extracts from HEK293 cells transfected with the indicated wild-type or mutant HA-tagged constructs and wild-type Cmyc-tagged constructs (ratio 1:2). The lower panel shows RAD51 co-immunoprecipitation with anti-Cmyc beads. A89E and R250A were used as experimental controls. EGFP-Cmyc is used as a negative control. (**C**) Quantification of the relative co-immunoprecipitation (coIP) efficiency of the RAD51-WT-Cmyc and mutant RAD51-HA (white bars), normalized to the relative coIP efficiency of the RAD51-WT-Cmyc and RAD51-WT-HA condition (black bar; n ≧ 3). For each condition, the IP efficiency was calculated as the ratio of IP normalized to Input RAD51 densities both for the prey (HA) and the gait (Cmyc) RAD51 proteins. Then the relative co-IP efficiency of each condition, i.e. the prey (HA) normalized with the gait (Cmyc) IP efficiencies, further normalized with the WT prey (HA) condition, was calculated for each experiment. Data are represented as means ± S.E.M. Significance was calculated by one-way ANOVA followed by Dunnett's *post hoc* test (**P*< 0.05, ***P*< 0.01, ****P*< 0.001).

Figure 5. Functional impact of *RAD51* pathogenic variants on RAD51 polymerization.
(**A-C**) Nucleofilament formation. Dark-field electron microscopy (EM) images of filaments formed by WT and/or mutant recombinant RAD51 proteins on (**A**) double-stranded DNA (linearized pBR322 – 4361 bp) or (**B, C**) single-stranded DNA (PhiX174 virion – 5386 nt). Insets in Ab,e show bright-field images of filaments formed in the same condition. In **A-B**, the nt/protein ratio was 3:1 for WT or mutant RAD51; in **C**, the nt/protein ratio for each indicated RAD51 protein was 6:1, resulting in equimolar ratio of WT and mutant RAD51 in Cb-d; in **B-C**, RPA protein (nt/protein ratio 100:1) was added to promote unfolding of the single-stranded DNA substrate and allow elongation of the nucleofilament. Inset in Ba shows single-stranded DNA without RPA. Scale bar represents 100 nm. (**D**) DNA binding assay. Representative electrophoretic migration shift assay (EMSA) of a Cy5-labeled single-strand DNA substrate after incubation with WT and/or mutant RAD51 recombinant proteins (same nt/protein ratio as in B-C). (**E-G**) Displacement loop (D-loop) activity. (**E**) Scheme of the D-loop assay. Filaments are formed on a 400-nt long ssDNA in presence of WT and/or mutant RAD51 recombinant proteins (as in D), followed by addition of a homologous supercoiled double-stranded DNA and deproteinization of the sample. (**F**) Representative electrophoretic gel of D-loop assay. (**G**) Quantification of the percentage of D-loop yield (n=3). Data are represented as means ± S.E.M. Significance was calculated by one-way ANOVA followed by Dunnett's *post hoc* test (**P*< 0.05, ***P*< 0.01, ****P*< 0.001).

Figure 1.

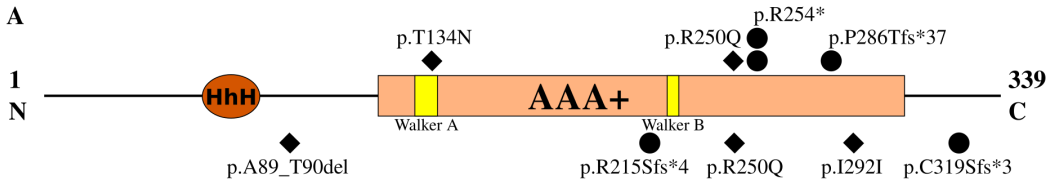
A
1
N
339
C
HhH
AAA+
Walker A
Walker B
p.T134N
p.R254*
p.R250Q
p.P286Tfs*37
p.A89_T90del
p.R215Sfs*4
p.R250Q
p.I292I
p.C319Sfs*3

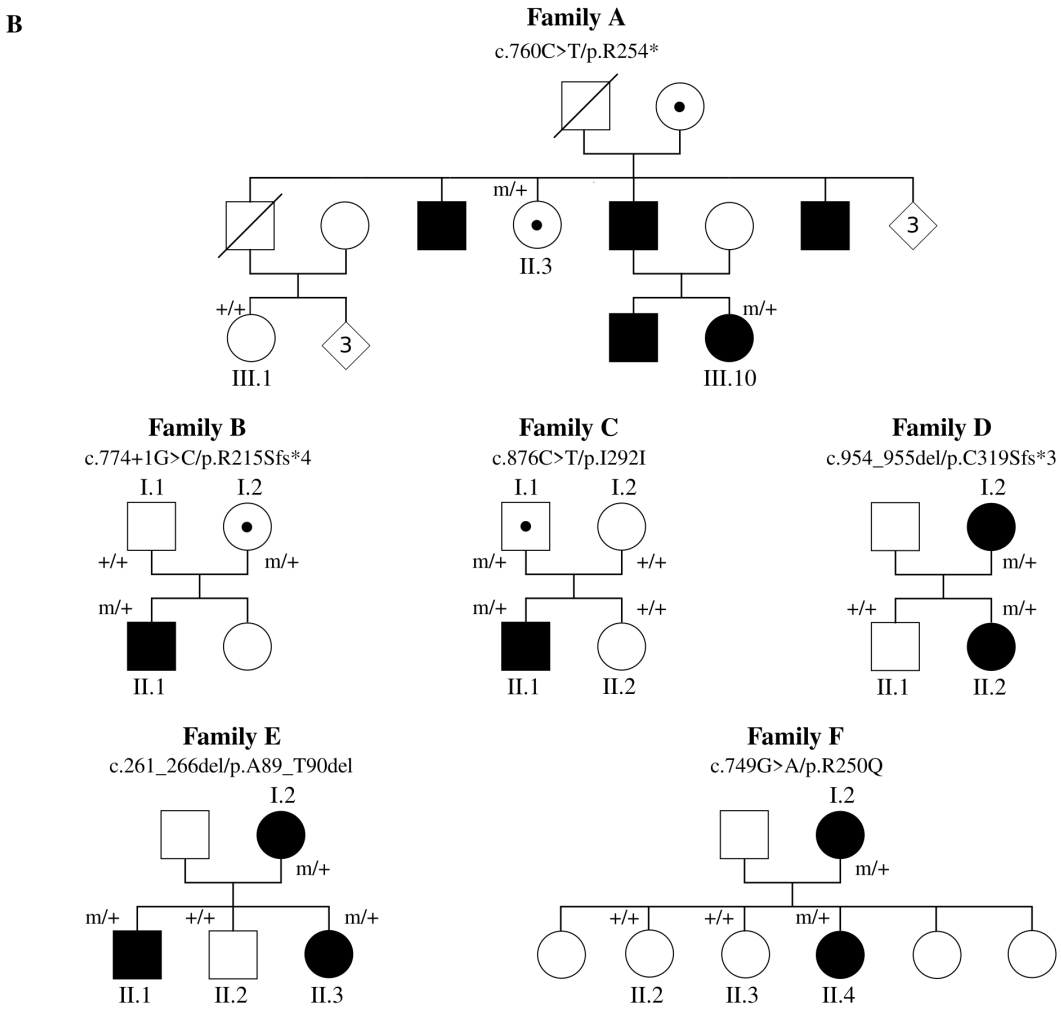
B
Family A
c.760C>T/p.R254*
m/+
II.3
3
+/+
3
III.1
m/+
III.10
Family B
c.774+1G>C/p.R215Sfs*4
I.1
I.2
+/+
m/+
m/+
II.1
Family C
c.876C>T/p.I292I
I.1
I.2
m/+
+/+
m/+
+/+
II.1
II.2
Family D
c.954_955del/p.C319Sfs*3
I.2
m/+
+/+
m/+
II.1
II.2
Family E
c.261_266del/p.A89_T90del
I.2
m/+
m/+
+/+
m/+
II.1
II.2
II.3
Family F
c.749G>A/p.R250Q
I.2
m/+
+/+
+/+
m/+
II.2
II.3
II.4

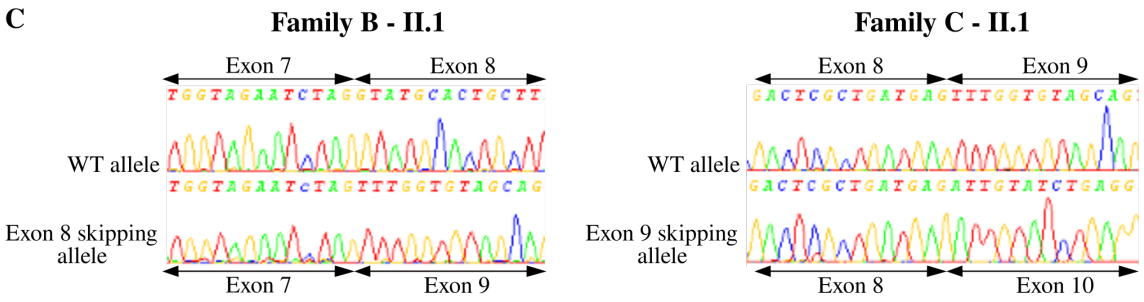
C
Family B - II.1
Exon 7
Exon 8
WT allele
Exon 8 skipping allele
Exon 7
Exon 9
Family C - II.1
Exon 8
Exon 9
WT allele
Exon 9 skipping allele
Exon 8
Exon 10


D
Empty
WT
c.774+1G>C
Empty
WT
c.876C>T
c.896+1G>A

Figure 2.

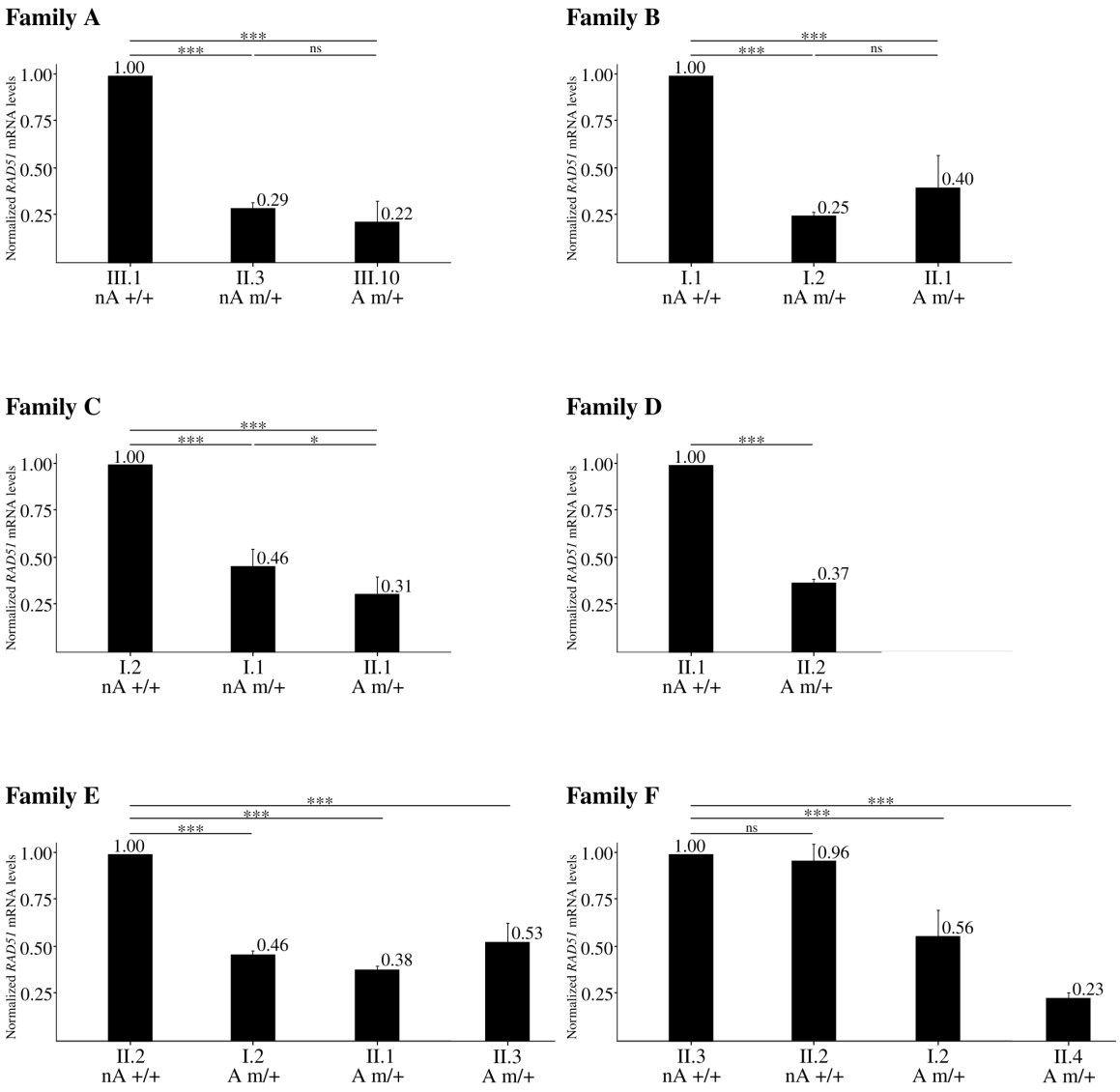
Family A
***
***
ns
Normalized RAD51 mRNA levels
1.00
0.75
0.50
0.25
1.00
0.29
0.22
III.1
nA +/+
II.3
nA m/+
III.10
A m/+
Family B
***
***
ns
1.00
0.25
0.40
I.1
nA +/+
I.2
nA m/+
II.1
A m/+
Family C
***
***
*
1.00
0.46
0.31
I.2
nA +/+
I.1
nA m/+
II.1
A m/+
Family D
***
1.00
0.37
II.1
nA +/+
II.2
A m/+
Family E
***
***
***
1.00
0.46
0.38
0.53
II.2
nA +/+
I.2
A m/+
II.1
A m/+
II.3
A m/+
Family F
***
***
ns
1.00
0.96
0.56
0.23
II.3
nA +/+
II.2
nA +/+
I.2
A m/+
II.4
A m/+

Figure 3. ■WT RAD51 protein □Mutant RAD51 protein ▩Total RAD51 protein

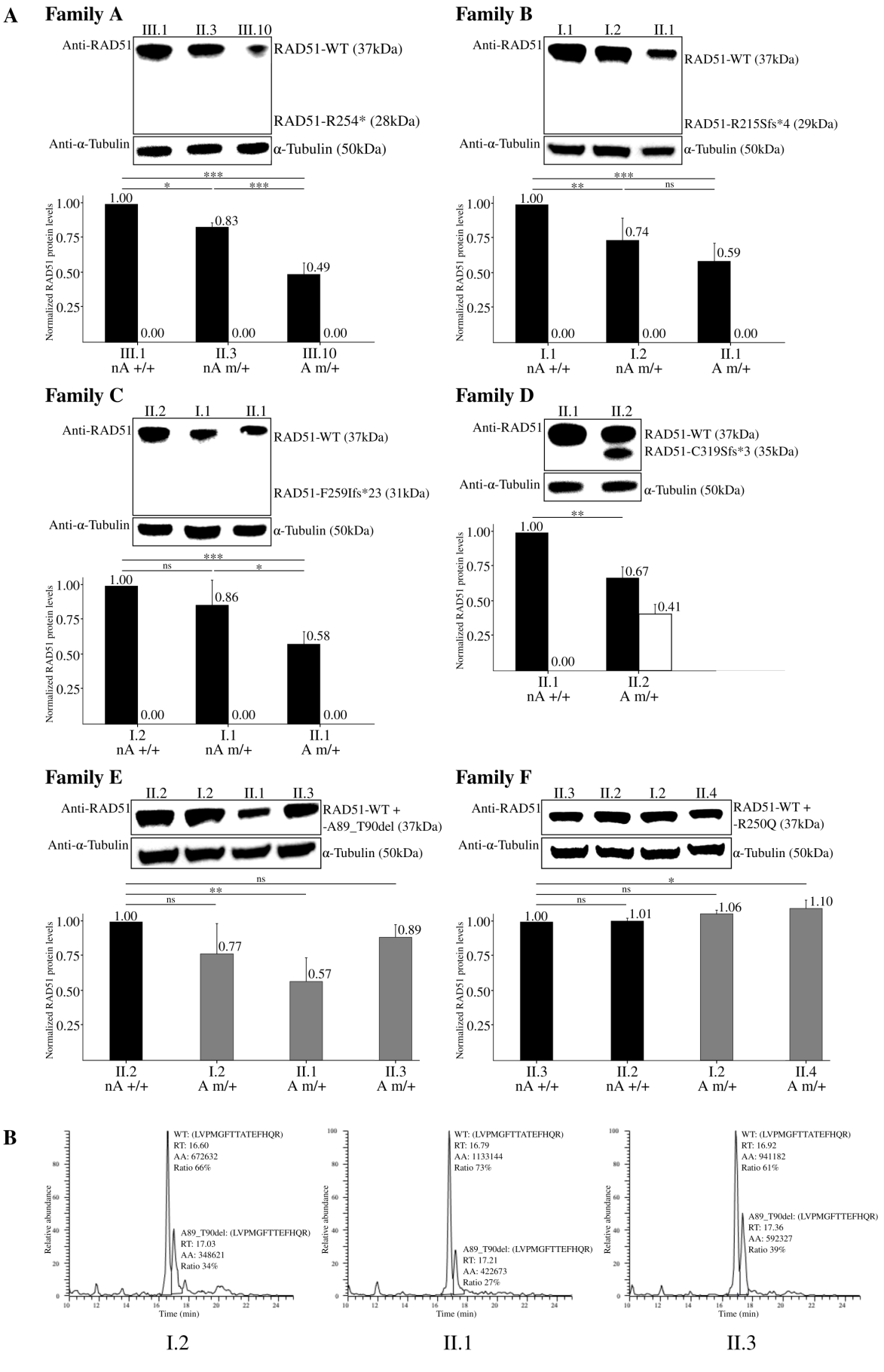

Figure 4.

A

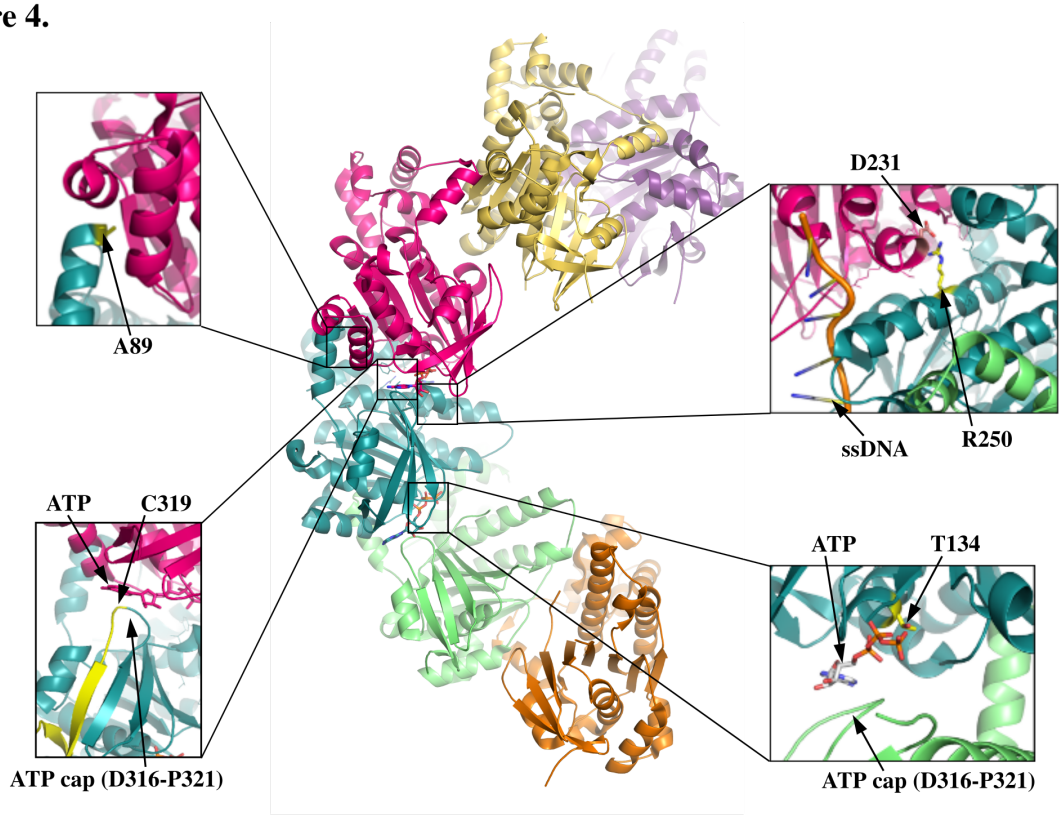
A89
D231
ssDNA
R250
ATP
C319
ATP cap (D316-P321)
ATP
T134
ATP cap (D316-P321)

B

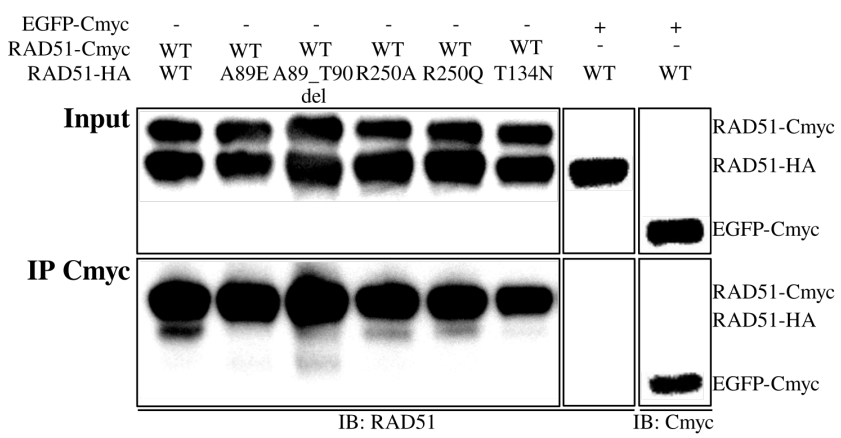
EGFP-Cmyc - - - - - - + +
RAD51-Cmyc WT WT WT WT WT WT - -
RAD51-HA WT A89E A89_T90del R250A R250Q T134N WT WT
Input
IP Cmyc
RAD51-Cmyc
RAD51-HA
EGFP-Cmyc
IB: RAD51
IB: Cmyc

C

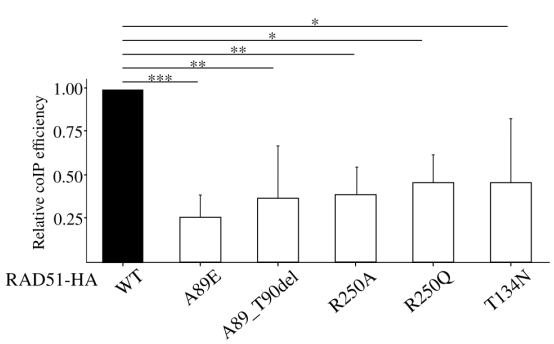
Relative coIP efficiency
1.00
0.75
0.50
0.25
RAD51-HA
WT
A89E
A89_T90del
R250A
R250Q
T134N

Figure 5.

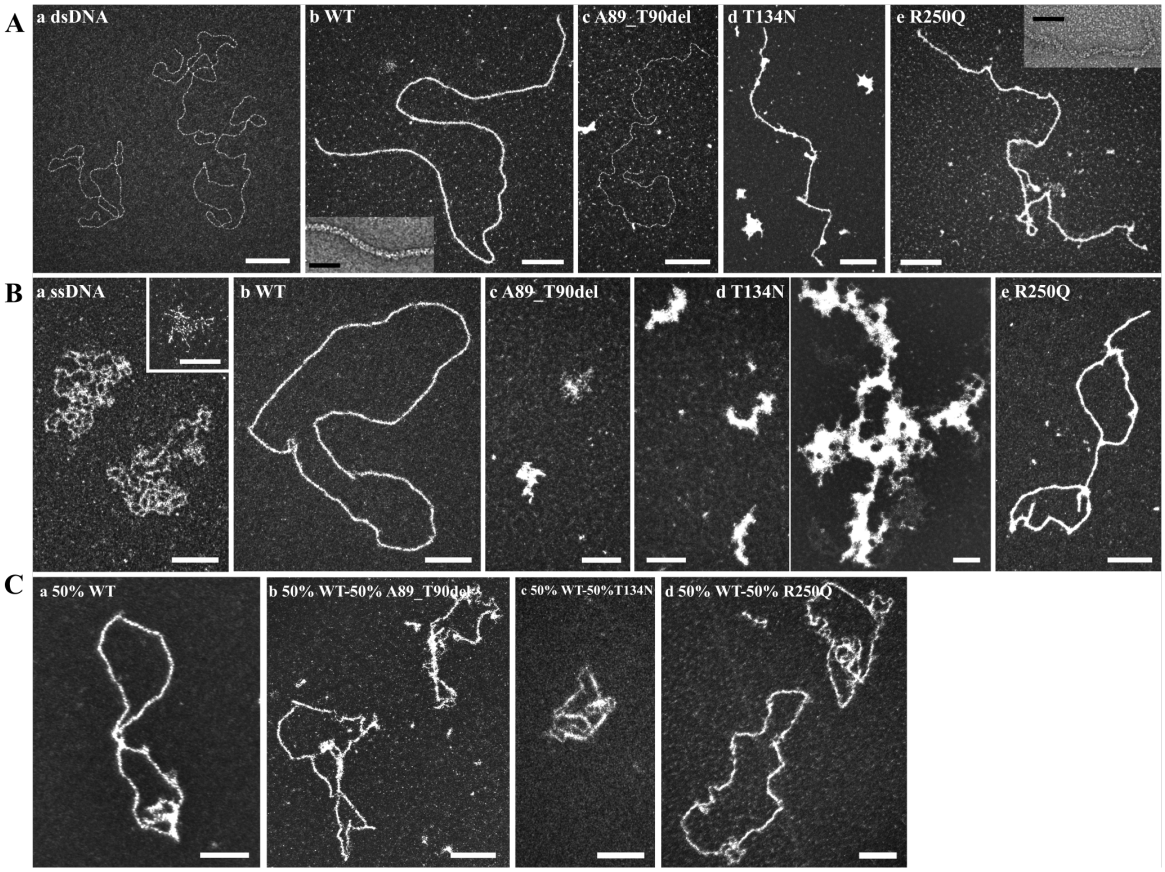
A
a dsDNA
b WT
c A89_T90del
d T134N
e R250Q
B
a ssDNA
b WT
c A89_T90del
d T134N
e R250Q
C
a 50% WT
b 50% WT-50% A89_T90del
c 50% WT-50%T134N
d 50% WT-50% R250Q

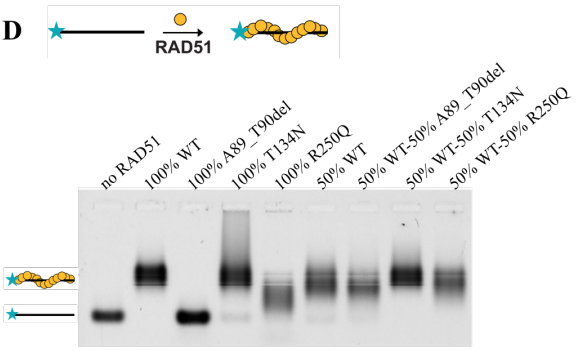
D
RAD51
no RAD51
100% WT
100% A89_T90del
100% T134N
100% R250Q
50% WT
50% WT-50% A89_T90del
50% WT-50% T134N
50% WT-50% R250Q

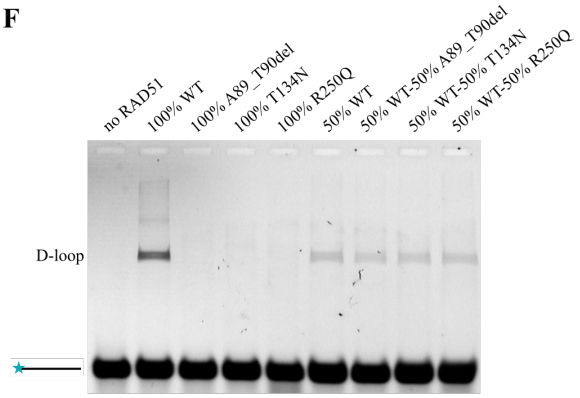
F
no RAD51
100% WT
100% A89_T90del
100% T134N
100% R250Q
50% WT
50% WT-50% A89_T90del
50% WT-50% T134N
50% WT-50% R250Q
D-loop

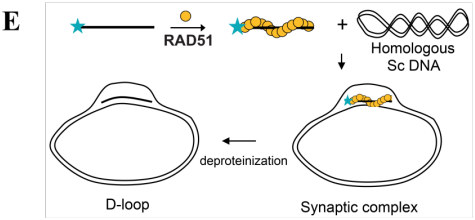
E
RAD51
Homologous
Sc DNA
deproteinization
D-loop
Synaptic complex

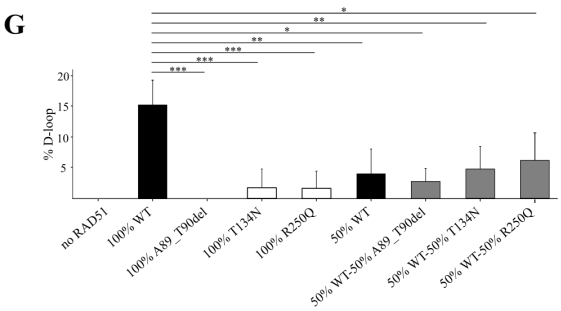
G
% D-loop
20
15
10
5
no RAD51
100% WT
100% A89_T90del
100% T134N
100% R250Q
50% WT
50% WT-50% A89_T90del
50% WT-50% T134N
50% WT-50% R250Q

LEGENDS OF THE SUPPLEMENTARY FIGURES.

Figure S1. Identification of the *RAD51* pathogenic variants in the six CMM families, and conservation of the altered amino acids in vertebrate RAD51 orthologous proteins.
(**A**) Genomic DNA sequence of *RAD51* heterozygous pathogenic variants in CMM index cases. For each family, the patient's electrophoregram (lower panel) is compared with the WT electrophoregram of an unaffected relative (upper panel). The red arrow points to sequence changes. (**B**) Partial alignments of RAD51 proteins across all vertebrate species showing full conservation of the amino acids altered in these CMM families. Multiple pairwise alignments were performed using Clustal Omega (*http://www.ebi.ac.uk/Tools/msa/clustalo/*). Amino acids altered by the pathogenic variation are boxed. Asterisk indicates a fully conserved residue; colon indicates conservation between groups of strongly similar properties; period indicates conservation between groups of weakly similar properties.

Figure S2. Expression of WT and mutant *RAD51* mRNAs in CMM families by ddPCR.
RNAs were extracted from the patients' lymphoblasts and *RAD51* mRNA expression was quantified by Droplet Digital PCR (ddPCR). Histograms in black correspond to WT *RAD51* mRNA and in white to mutant *RAD51* mRNA (for Family C, white to *I292I* mRNA and grey to exon 9 skipping mRNA). A, affected; nA, non-affected; m, mutated allele; +, wild-type allele.

Figure S3. Expression of mutant *RAD51* mRNA in CMM families.
For each individual of a given family, the mutant *RAD51* mRNA levels were quantified by allele specific RT-qPCR and normalized to the WT allele of the non-mutated relative ($n \geqq 3$). Data are represented as means ± S.E.M. Significance was calculated by two-way ANOVA followed by Tukey's *post hoc* test (ns, non-significant; $***P < 0.001$). A, affected; nA, non-affected; m, mutated allele; +, wild-type allele.

Figure S4. NMD targeting of the new truncating RAD51 pathogenic variants.
Lymphoblastic cells from individuals of Families B, C and D were treated with 10 mg/mL emetin (+ emetin), to inhibit nonsense-mediated mRNA decay (NMD), or not (- emetin). RNAs were extracted and *RAD51* fragments spanning the exon skipped in the mutant allele (Families B and C) or including the variant region (Family D) were amplified by RT-PCR. Representative electrophoresis result (Families B and C) or electropherograms (Family D) show the RT-PCR products, separation on agarose gel or after sequencing respectively. A, affected; nA, non-affected; m, mutated allele; +, wild-type allele.

Figure S5. Expression levels of WT or mutant RAD51 proteins.
Levels of WT or mutant RAD51 proteins were quantified in the patients' lymphoblasts by western blot (Families A-D) or by a combination of western blot and mass spectrometry (Family E) and represented as a percentage of intrafamilial healthy individuals. For Family F, WT and mutant proteins could not be distinguished and total RAD51 protein levels were quantified by western blot. The threshold under which WT RAD51 levels are pathogenic is indicated. Histograms in black correspond to WT RAD51 proteins; in white to mutant RAD51 proteins; in grey to total RAD51 proteins. A, affected; nA, non-affected; m, mutated allele; +, wild-type allele. See Figure 3 for raw data.

Figure S6. Low expression of a RAD51 alternative isoform across CMM families.
Representative immunoblot performed on whole cell protein extracts from the patients' lymphoblasts. At longer exposure time, a 31-kDa band was observed for Family C members, both in mutated patients (lanes 2 and 3) and their healthy relative (lane 1), that may correspond

to the exon 9 skipping isoform of the RAD51 protein. A similar 31-kDa band was also observed in the non-mutated relatives of other families (lanes 4-7). A, affected; nA, non-affected; m, mutated allele; +, wild-type allele.

Figure S7. Instability of the RAD51-C319Sfs*3 protein.
(**A**) Representative immunoblot performed on whole cell protein extracts from HEK293T cells transfected with RAD51-WT-Cmyc and RAD51-C319Sfs*3-HA constructs in absence (- CHX) or presence of cycloheximide treatment (CHX, 10 μg/mL) for the indicated duration. Upper panel shows lower levels of RAD51-C319Sfs*3 as compared with RAD51-WT at the latter timepoint. Lower panel: α-Tubulin, used as a loading control. (**B**) Quantification of the relative protein levels in the CHX vs. - CHX conditions for RAD51-C319Sfs*3 protein (open symbols) compared to RAD51-WT protein (black symbols; $n = 3$). Data are represented as means ± S.E.M. Significance was calculated by two-way ANOVA.

Figure S1.

A

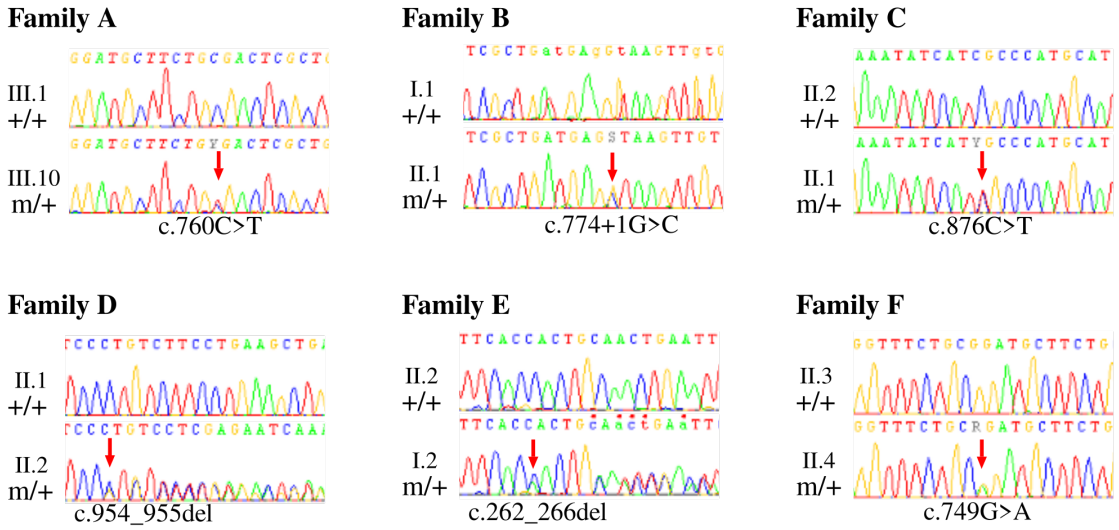

B

```
                                                    A89_T90del
RAD51_Human              PKKELINIKGISEAKADKILAEAAKLVPMGFTTATEFHQRRSEIIQITTGSKELDKLLQG   115
RAD51_Macaque            PKKELINIKGISEAKADKILAEAAKLVPMGFTTATEFHQRRSEIIQITTGSKELDKLLQG   115
RAD51_Vervet-AGM         PKKELINIKGISEAKADKILAEAAKLVPMGFTTATEFHQRRSEIIQITTGSKELDKLLQG   115
RAD51_Mouse              PKKELINIKGISEAKADKILTEAAKLVPMGFTTATEFHQRRSEIIQITTGSKELDKLLQG   115
RAD51_Rat                PKKELINIKGISEAKADKILAEAAKLVPMGFTTATEFHQRRSEIIQITTGSKELDKLLQG   115
RAD51_Cow                PKKELINIKGISEAKADKILTEAAKLVPMGFTTATEFHQRRSEIIQITTGSKELDKLLQG   115
RAD51_Dog                PKKELISIKGISEAKADKILTEAAKLVPMGFTTATEFHQRRSEIIQITTGSKELDKLLQG   115
RAD51_Chicken            PKKELLNIKGISEAKADKILAEAAKLVPMGFTTATEFHQRRSEIIQITTGSKELDKLLQG   115
RAD51_Anole-lizard       PKKELLNIKGISEAKADKILAEAAKLVPMGFTTATEFHQQRSEIIQITTGSKELDKLLQG   120
RAD51_Zebrafish          PKKELLNIKGISEAKADKILTEAAKMVPMGFTTATEFHQRRAEIIQISTGSKELDKLLQG   116
RAD51_Tetraodon          PKKELLNIKGISEAKADKILTEAAKLVPMGFTTATEFHQRRAEIIQISTGSKELDKLLQG   116
                         *****:.*************:****:*************:*:*****:************

                                                    R215Sfs*4
RAD51_Human              ERYGLSGSDVLDNVAYARAFNTDHQTQLLYQASAMMVESRYALLIVDSATALYRTDYSGR   235
RAD51_Macaque            ERYGLSGSDVLDNVAYARAFNTDHQTQLLYQASAMMVESRYALLIVDSATALYRTDYSGR   235
RAD51_Vervet-AGM         ERYGLSGSDVLDNVAYARAFNTDHQTQLLYQASAMMVESRYALLIVDSATALYRTDYSGR   235
RAD51_Mouse              ERYGLSGSDVLDNVAYARGFNTDHQTQLLYQASAMMVESRYALLIVDSATALYRTDYSGR   235
RAD51_Rat                ERYGLSGSDVLDNVAYARGFNTDHQTQLLYQASAMMVESRYALLIVDSATALYRTDYSGR   235
RAD51_Cow                ERYGLSGSDVLDNVAYARGFNTDHQTQLLYQASAMMVESRYALLIVDSATALYRTDYSGR   235
RAD51_Dog                ERYGLSGSDVLDNVAYARGFNTDHQTQLLYQASAMMVESRYALLIVDSATALYRTDYSGR   235
RAD51_Chicken            ERYGLSGSDVLDNVAYARGFNTDHQTQLLYQASAMMAESRYALLIVDSATALYRTDYSGR   235
RAD51_Anole-lizard       ERYGLSGSDVLDNVAYARGFNTDHQTQLLYQASAMMTESRYALLIVDSATALYRTDYSGR   240
RAD51_Zebrafish          ERYGLVGSDVLDNVAYARAFNTDHQTQLLYQASAMMTESRYALLIVDSATALYRTDYSGR   236
RAD51_Tetraodon          ERYGLVGSDVLDNVAYARAFNTDHQTQLLYQASAMMAESRYALLIVDSATALYRTDYSGR   236
                         ***** ***********.*****************.**********************

                           R250Q  R254*
RAD51_Human              GELSARQMHLARFLRMLLRLADEFGVAVVITNQVVAQVDGAAMFAADPKKPIGGNIIAHA   295
RAD51_Macaque            GELSARQMHLARFLRMLLRLADEFGVAVVITNQVVAQVDGAAMFAADPKKPIGGNIIAHA   295
RAD51_Vervet-AGM         GELSARQMHLARFLRMLLRLADEFGVAVVITNQVVAQVDGAAMFAADPKKPIGGNIIAHA   295
RAD51_Mouse              GELSARQMHLARFLRMLLRLADEFGVAVVITNQVVAQVDGAAMFAADPKKPIGGNIIAHA   295
RAD51_Rat                GELSARQMHLARFLRMLLRLADEFGVAVVITNQVVAQVDGAAMFAADPKKPIGGNIIAHA   295
RAD51_Cow                GELSARQMHLARFLRMLLRLADEFGVAVVITNQVVAQVDGAAMFAADPKKPIGGNIIAHA   295
RAD51_Dog                GELSARQMHLARFLRMLLRLADEFGVAVVITNQVVAQVDGAAMFAADPKKPIGGNIIAHA   295
RAD51_Chicken            GELSARQMHLARFLRMLLRLADEFGVAVVITNQVVAQVDGAAMFAADPKKPIGGNIIAHA   295
RAD51_Anole-lizard       GELSARQMHLARFLRMLLRIADEFGVAVVITNQVVAQVDGAAMFAADPKKPIGGNIIAHA   300
RAD51_Zebrafish          GELSARQGHLGRFLRMLLRLADEFGVAVVITNQVVAQVDGAAMFSADPKKPIGGNILAHA   296
RAD51_Tetraodon          GELSARQGHLGRFLRMLLRLADEFGVAVVITNQVVAQVDGAAMFSADPKKPIGGNILAHA   296
                         ******* **.********:**********************:***********:***

                                                    C319Sfs*3
RAD51_Human              STTRL-YLRKGRGETRICKIYDSPCLPEAEAMFAINADGVGDAKD   339
RAD51_Macaque            STTRL-YLRKGRGETRICKIYDSPCLPEAEAMFAINADGVGDAKD   339
RAD51_Vervet-AGM         STTRL-YLRKGRGETRICKIYDSPCLPEAEAMFAINADGVGDAKD   339
RAD51_Mouse              STTRL-YLRKGRGETRICKIYDSPCLPEAEAMFAINADGVGDAKD   339
RAD51_Rat                STTRL-YLRKGRGETRICKIYDSPCLPEAEAMFAINADGVGDAKD   339
RAD51_Cow                STTRL-YLRKGRGETRICKIYDSPCLPEAEAMFAINADGVGDAKD   339
RAD51_Dog                STTRW-SGRCQR-----LKHWGLSCEKP-----------------   317
RAD51_Chicken            STTRL-YLRKGRGETRICKIYDSPCLPEAEAMFAINADGVGDAKE   339
RAD51_Anole-lizard       STTRL-YLRKGRGETRICKIYDSPCLPEAEAMFAINPDGIGDAKD   344
RAD51_Zebrafish          STTRL-YLRKGRGETRICKIYDSPCLPEAEAMFAINADGVGDAKD   340
RAD51_Tetraodon          STTRFCTLRKGRGETRICKIYDSPCLPEAEAMFAINADGVGDAKD   341
                         ****    *  *      * :.  *
```

Figure S2.

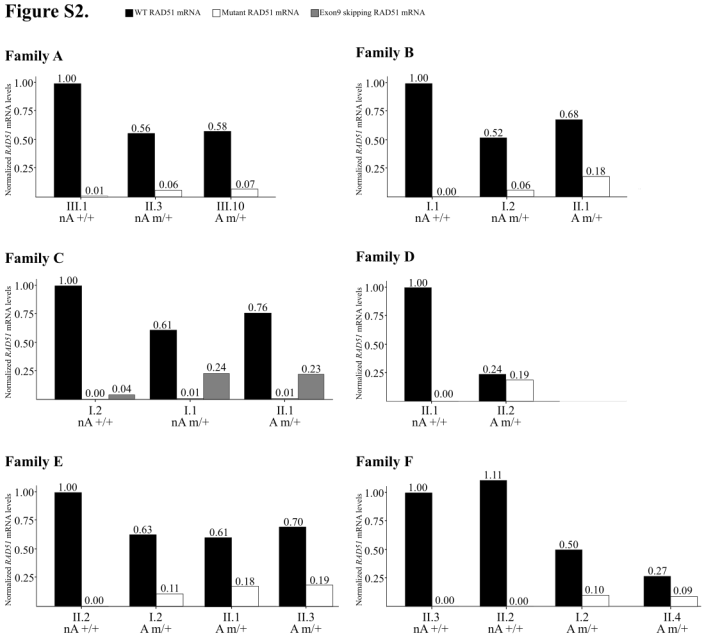
WT RAD51 mRNA
Mutant RAD51 mRNA
Exon9 skipping RAD51 mRNA
Family A
Normalized RAD51 mRNA levels
1.00
0.01
0.56
0.06
0.58
0.07
III.1 nA +/+
II.3 nA m/+
III.10 A m/+
Family B
1.00
0.00
0.52
0.06
0.68
0.18
I.1 nA +/+
I.2 nA m/+
II.1 A m/+
Family C
1.00
0.00
0.04
0.61
0.01
0.24
0.76
0.01
0.23
I.2 nA +/+
I.1 nA m/+
II.1 A m/+
Family D
1.00
0.00
0.24
0.19
II.1 nA +/+
II.2 A m/+
Family E
1.00
0.00
0.63
0.11
0.61
0.18
0.70
0.19
II.2 nA +/+
I.2 A m/+
II.1 A m/+
II.3 A m/+
Family F
1.00
0.00
1.11
0.00
0.50
0.10
0.27
0.09
II.3 nA +/+
II.2 nA +/+
I.2 A m/+
II.4 A m/+

Figure S3.

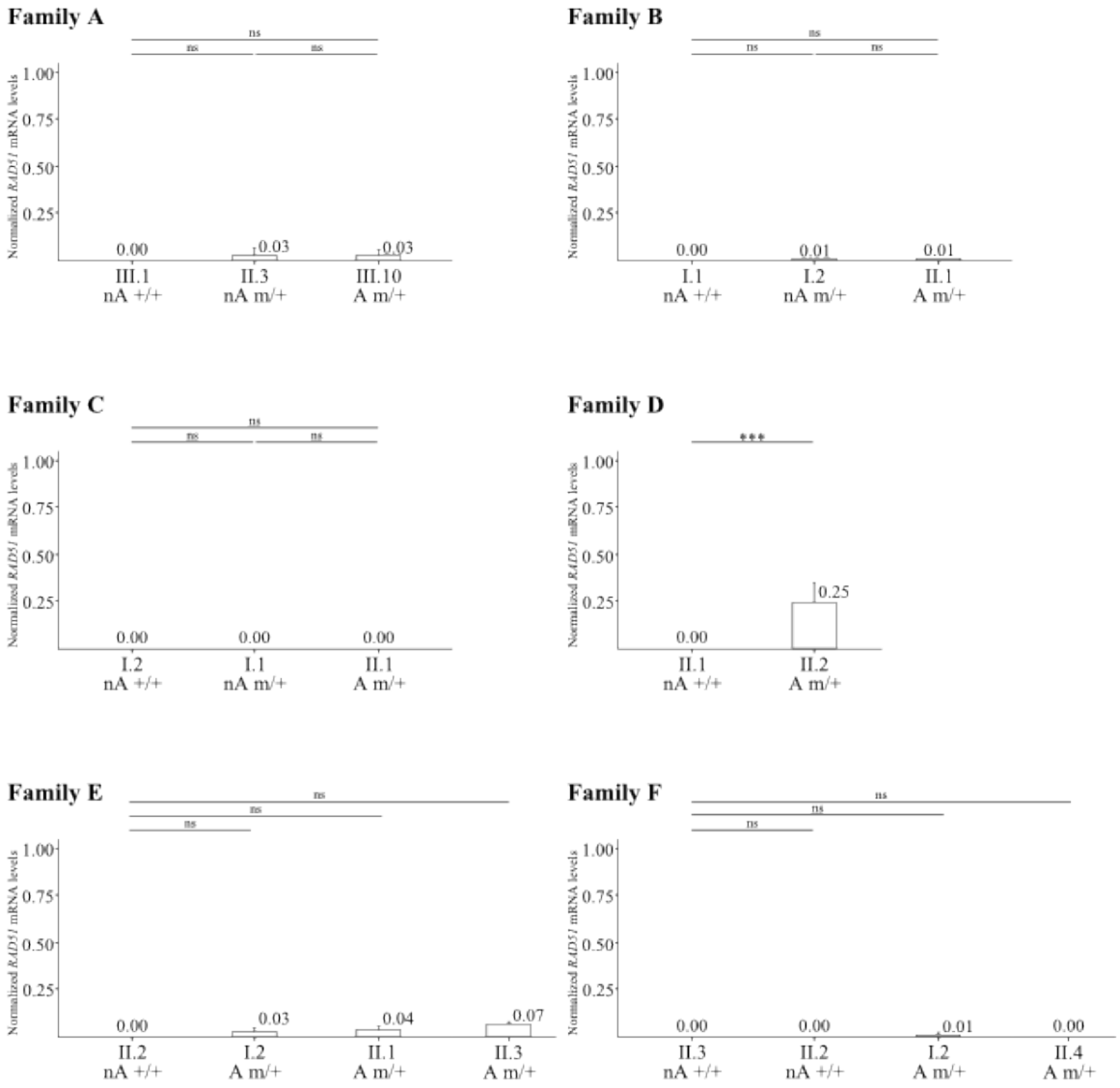
Family A
ns
ns
ns
Normalized RAD51 mRNA levels
1.00
0.75
0.50
0.25
0.00
0.03
0.03
III.1
nA +/+
II.3
nA m/+
III.10
A m/+
Family B
ns
ns
ns
Normalized RAD51 mRNA levels
1.00
0.75
0.50
0.25
0.00
0.01
0.01
I.1
nA +/+
I.2
nA m/+
II.1
A m/+
Family C
ns
ns
ns
Normalized RAD51 mRNA levels
1.00
0.75
0.50
0.25
0.00
0.00
0.00
I.2
nA +/+
I.1
nA m/+
II.1
A m/+
Family D
***
Normalized RAD51 mRNA levels
1.00
0.75
0.50
0.25
0.00
0.25
II.1
nA +/+
II.2
A m/+
Family E
ns
ns
ns
Normalized RAD51 mRNA levels
1.00
0.75
0.50
0.25
0.00
0.03
0.04
0.07
II.2
nA +/+
I.2
A m/+
II.1
A m/+
II.3
A m/+
Family F
ns
ns
ns
Normalized RAD51 mRNA levels
1.00
0.75
0.50
0.25
0.00
0.00
0.01
0.00
II.3
nA +/+
II.2
nA +/+
I.2
A m/+
II.4
A m/+

Figure S4.

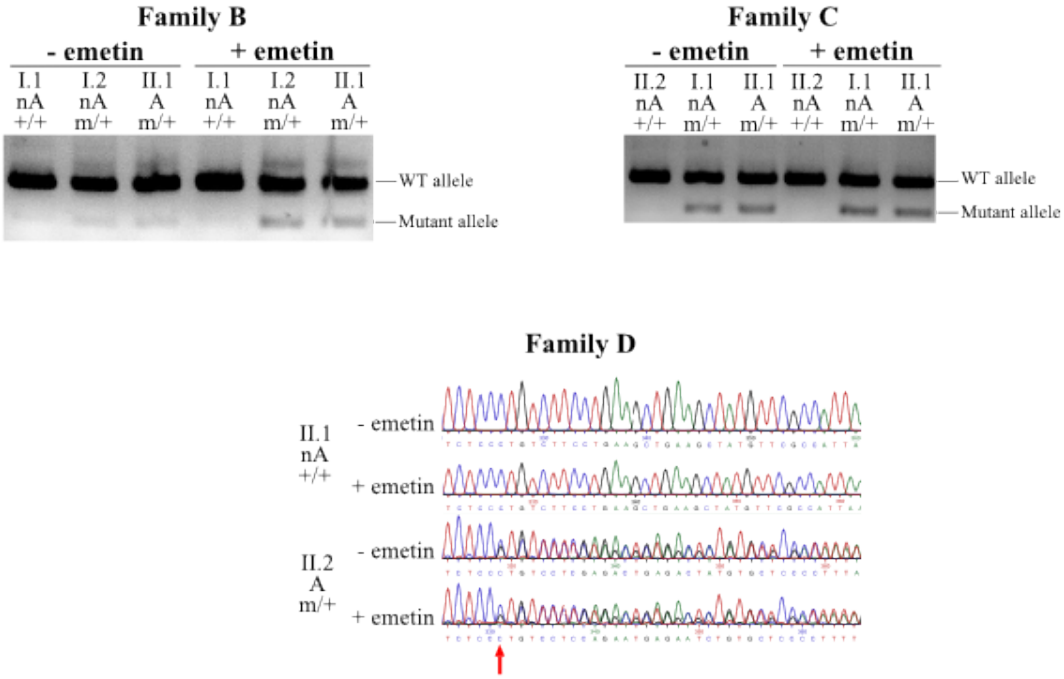
Family B
- emetin
+ emetin
I.1 nA +/+
I.2 nA m/+
II.1 A m/+
I.1 nA +/+
I.2 nA m/+
II.1 A m/+
WT allele
Mutant allele
Family C
- emetin
+ emetin
II.2 nA +/+
I.1 nA m/+
II.1 A m/+
II.2 nA +/+
I.1 nA m/+
II.1 A m/+
WT allele
Mutant allele
Family D
II.1 nA +/+
- emetin
+ emetin
II.2 A m/+
- emetin
+ emetin

Figure S5.

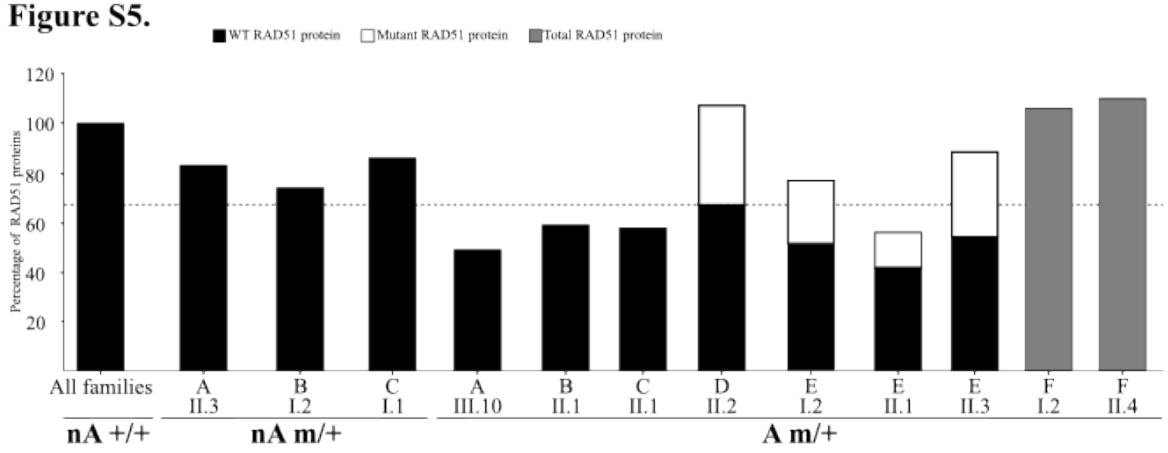
WT RAD51 protein
Mutant RAD51 protein
Total RAD51 protein
Percentage of RAD51 proteins
120
100
80
60
40
20
All families
A II.3
B I.2
C I.1
A III.10
B II.1
C II.1
D II.2
E I.2
E II.1
E II.3
F I.2
F II.4
nA +/+
nA m/+
A m/+

Figure S6.

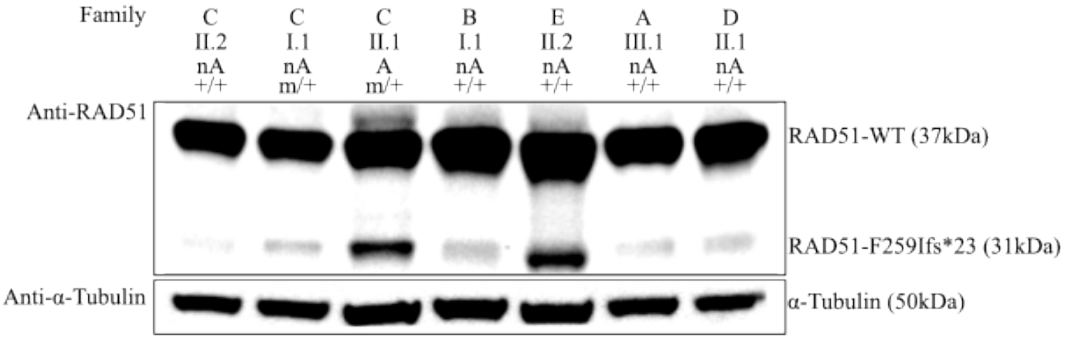
Family
C II.2 nA +/+
C I.1 nA m/+
C II.1 A m/+
B I.1 nA +/+
E II.2 nA +/+
A III.1 nA +/+
D II.1 nA +/+
Anti-RAD51
RAD51-WT (37kDa)
RAD51-F259Ifs*23 (31kDa)
Anti-α-Tubulin
α-Tubulin (50kDa)

Figure S7.

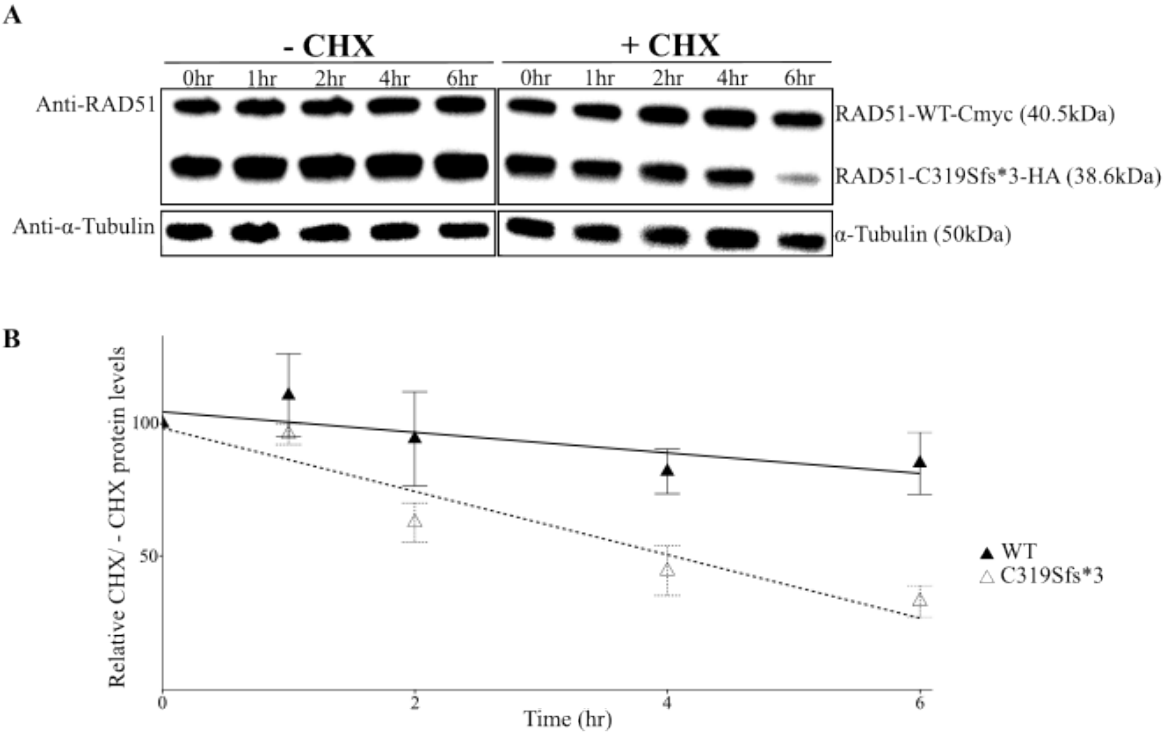
A
- CHX
+ CHX
0hr 1hr 2hr 4hr 6hr
0hr 1hr 2hr 4hr 6hr
Anti-RAD51
RAD51-WT-Cmyc (40.5kDa)
RAD51-C319Sfs*3-HA (38.6kDa)
Anti-α-Tubulin
α-Tubulin (50kDa)
B
Relative CHX/ - CHX protein levels
100
50
0
2
4
6
Time (hr)
▲ WT
△ C319Sfs*3

SUPPLEMENTARY EXPERIMENTAL PROCEDURES

Digital droplet PCR (ddPCR).

QX200 ddPCR EvaGreen Supermix (Bio-Rad) was used to run the PCR reaction using the primers listed in Table S2. PCR conditions were: 95°C for 5 min, 40 cycles of 95°C for 30 s / 60°C for 1 min. Droplets generated with the Bio-Rad QX100 Droplet Generator were analyzed using the Bio-Rad QX200 Droplet Reader and QuantaSoft software (Bio-Rad).

RAD51 constructs for transfection.

RAD51 constructs were derived from the Cmyc-tagged wild-type (WT) human *RAD51* cDNA (NCBI Reference Sequence: NM_002875) in the pCMV6-Entry backbone (Origene). Primers used for the mutagenesis or amplification steps are listed in Table S2. *RAD51* mutations were introduced in the RC218333 plasmid with QuikChange Lightning Site-Directed Mutagenesis Kit (Agilent Technologies). The EGFP sequence was amplified and cloned into BamHI/NotI digested RC218333 plasmid with NEBuilder HiFi DNA Assembly Cloning Kit (New England BioLabs). The WT and mutant *RAD51* sequences were then amplified and cloned in SacI/NotI digestion of a pCAGGs-HA plasmid (derived from Addgene) with the same kit. For the minigene experimental splicing assay, WT and mutant *RAD51* genomic fragments were amplified from the patients' genomic DNA and inserted into the BamHI/MluI sites of pCAS2 yielding pCAS2-RAD51 hybrid minigenes. The positive control carrying donor splice site variant c.896+1 G>A in *RAD51* exon 9 was obtained with QuikChange Lightning Site-Directed Mutagenesis Kit (Agilent Technologies).

Protein extraction and western blot.

Cells were lysed in lysis buffer (25 mM Tris [pH 7.5], 150 mM NaCl, 1% NP-40, 0.5% sodium deoxycholate, 1 mM EDTA and 5% glycerol). 25 µg of the samples were separated on 10% Bis-Tris NuPage gel (Thermo Fisher Scientific) and transferred onto PVDF membranes

(Millipore). After blocking in 1× TBS-T (2 mM Tris [pH 7.4], 150 mM NaCl, 0.05% Tween-20) supplemented with 5% (w/v) dried skim milk powder, the membranes were incubated with antibodies. All the antibodies used for western blots are listed in Table S3. Detection was performed using Pierce ECL Western Blotting Substrate (Thermo Fisher Scientific) with the ChemiDoc MP imaging system (Bio-Rad). Density was quantified using ImageJ software (NIH).

Cell treatments.

Emetin treatment: LCLs from individuals of families B, C and D were treated with 10 mg/mL emetin overnight (Sigma-Aldrich) to inhibit NMD.

Cycloheximide treatment: HEK293 cells were transfected with the adequate RAD51 constructs using Lipofectamine 2000 (Thermo Fisher Scientific). The day after, the cells were treated with 10 µg/mL cycloheximide (CHX, Sigma-Aldrich) for either 1, 2, 4 or 6 hrs. The cells were lysed as described above. Untreated cells were harvested at timepoint 0 as a reference point. 5 µg of protein were loaded on an SDS-gel followed by western blotting analysis as described above. Experiments consisted of three independent replicates. At each timepoint, the amounts of WT or mutated RAD51 proteins with or without CHX were quantified, and the ratio of proteins without CHX calculated to compare WT and mutated RAD51 turnovers.

Purification of RAD51 recombinant proteins.

Recombinant His-SUMO-RAD51 (1) was expressed in *E. coli* strain BRL (DE3) pLys. Cells from a 3-liter culture that was induced with 0.5 mM isopropyl-1-thio-ß-D-galactopyranoside overnight at 20°C were resuspended in 1× PBS, 350 mM NaCl, 20 mM imidazole, 10% glycerol, 0.5 mg/mL lysozyme, Complete Protease Inhibitor Cocktail (Roche), and 1 mM 4-(2-aminoethyl)-benzenesulfonyl fluoride (AEBSF). The cells were lysed by sonication and insoluble material was removed by centrifugation at 150,000 g for 1 hr. The supernatant was incubated with 5 mL of Ni-NTA resin (Qiagen) for 2 hrs. The mixture was poured into an

Econo-Column Chromatography Column (Bio-Rad) and the beads were washed first with W1 buffer (20 mM Tris HCl [pH 8], 500 mM NaCl, 20 mM imidazole, 10% glycerol, 0.5% NP40), followed by W2 buffer (20 mM Tris HCl [pH 8], 100 mM NaCl, 20 mM imidazole, 10% glycerol, 1 mM DTT). His-SUMO-RAD51 bound to the beads was then resuspended with 8 mL of W2 buffer and incubated with SUMO protease at a ratio of 1/80 (w/w) for 16 hrs. RAD51 without the His-SUMO tag was then recovered into the flow thru and directly loaded onto a HiTrap heparin column (GE Healthcare). The column was washed with W2 buffer and then a 0.1-1 M NaCl gradient was applied. Fractions containing purified RAD51 were concentrated and dialyzed against storage buffer (20 mM Tris HCl [pH 8], 50 mM KCl, 0.5 mM EDTA, 10% glycerol, 1 mM DTT, and 0.5 mM AEBSF).

Mass Spectrometry.

2.5 mg of cell lysate protein were immunoprecipitated with beads (Thermo Fisher Scientific) coated with RAD51 antibody (Table S3). Proteins were eluted with Lane Marker Reducing Buffer (Thermo Fisher Scientific) and were loaded on an SDS-gel as described above. The gel was stained with Page Blue TM Protein Staining Solution (Thermo Fisher Scientific). The stained gel pieces were excised, destained and reduced with 10 mM DTT, alkylated with 20 mM iodoacetamide and digested *in situ* overnight using trypsin. The digestion was quenched by adding 0.1% formic acid final concentration, followed by an extraction of peptides with 0.1% formic acid/acetonitrile (50/50 v/v) before being dried in a speed-vacuum. Half of the extracted peptide sample, in 0.1% formic acid, were loaded on an Evotip and injected for LC-MS/MS analysis. Digested peptides were analyzed on an Orbitrap Fusion mass spectrometer (Thermo Fisher Scientific) coupled with an Evosep one system operating with the 30SPD method. The Orbitrap Fusion was operated in PRM acquisition mode to automatically alternate between a MS1 scan (*m/z* range 350−2000) and subsequent HCD MS/MS PRM scans for two ions targeting WT and A89_T90del mutant $[M + H]^{3+}$ peptides of interest (*m/z* 578.959 and

521.598, respectively). The full scan event was performed at a *m/z* 300–2000 mass range, an orbitrap resolution of 120,000 (at *m/z* 200), a target automatic gain control (AGC) value of 4e5, and maximum ion accumulation time of 50 ms. PRM MS/MS scans were acquired in the ion trap with an isolation window of 1.6 Da and collision energy at 30% (HCD). The target AGC was set to 1e4 and the maximum ion accumulation time was 500 ms. Raw data were processed with the Thermo Xcalibur v3.0.63 software. XIC Peaks were integrated using the Genesis peak algorithm, a Boxcar smoothing value of 3 points, and enabling valley detection in peak detection settings. MSMS fragmentation data were acquired to confirm the peak identity by comparison with specific fragmentation spectra of WT and A89_T90del mutant peptides previously recorded from recombinant samples and analyzed with the Peaks Studio Xpro software (Bioinformatics Solutions Inc).

SUPPLEMENTARY TABLES

Table S1. Characteristics of patients with *RAD51* pathogenic variants.

Family	A[e]	B	C	D		E			F	
Geographic origin	French	Danish	French	French		French			French	
Affected individual	III.10	II.1	II.1	I.2	II.2	I.2	II.1	II.3	I.2	II.4
Sex/Age range (years)[a]	F/25-29	M/5-9	M/30-34	F/40-44	F/10-14	F/25-29	M/5-9	F/0-4	F/40-44	F/10-14
MM severity[b]/location	3/hands, forearms, 1/feet	3/hands, 2/feet	3/hands, forearms	1/hands	2/hands, 2/feet	3/hands	2/hands	3/hands	2/hands	3/hands
Brain MRI	Normal	Normal	Normal	ND	Normal	Normal	ND	ND	ND	ND
Functional disability	Difficulties in fine bimanual activities, pain/cramp during sustained manual activities, writing fatigability	no	Difficulties in fine bimanual activities	no	Difficulties in fine bimanual activities, writing fatigability	Difficulties in fine bimanual activities	no	Difficulties in fine bimanual activities	no	no
Variant: genomic description[c]	g.40729620C>T	g.40729635G>C	g.40729954C>T	g.40731112_40731113del		g.40706212_40706217del			g.40729609G>A[f]	
transcript description[c]	c.760C>T	c.774+1G>C	c.876C>T	c.954_955del		c.261_266del			c.749G>A[f]	
Protein change[c]	p.(R254*)	p.(R215Sfs*4)	p.(I292=)	p.(C319Sfs*3)		p.(A89_T90del)			p.(R250Q)[f]	
Predicted consequences	Nonsense, expect NMD	Frameshift, expect NMD	Synonymous	Frameshift, last exon, escape NMD		In-frame deletion			Missense	
***In-silico* predictions:**										
SIFT	n.a.	n.a.	n.a.	n.a		n.a.			Deleterious	
PolyPhen-2	n.a.	n.a.	n.a.	n.a.		n.a.			Possibly damaging	
CADD	40	34	8.316	33		18			32	
Allele frequency[d]	$7.423.10^{-6}$	0	0	0		0			0	
ACMG Classification	Pathogenic (PVS1, PM2, PP1, PP4)	Pathogenic (PVS1, PM2, PP4)	VUS (PM2, PP4)	Likely pathogenic (PVS1_strong, PM2, PP1, PP4)		Likely pathogenic (PM2, PM4, PP1, PP4)			Likely pathogenic (PM2, PP1, PP3, PP4, PP5)	

F, female; M, male; ND: no data; NMD, nonsense-mediated decay; n.a., not applicable; SIFT, Sorting Intolerant From Tolerant; PolyPhen-2, Polymorphism Phenotyping v2; CADD, Combined Annotation Dependent Depletion; ACMG, American College of Medical Genetics and Genomics. [a] Age at diagnosis; [b] The severity of MMs was evaluated with the Woods and Teuber rating scale (2); [c] HGVS nomenclature, based on GRCh38 (hg38), NM_002875.5 and NP_002866; [d] Allele frequency in gnomAD, Genome Aggregation Database v3.1.2; non-neuro; [e] Family already studied in (3); [f] Same variant as in (4).

Table S2. List of primers used in this study.

Primer name	Sequence 5'_3'
Primers used to amplify the coding and flanking regions of RAD51 (PCR)	
RAD51-Exon2_For	CGACTAGCTAGATAGAAGATGGGG
RAD51-Exon2_For	GGTCTTGACCTTGGTAGTAAACC
RAD51-Exon3_For	ACAAGTCTTCAAGCACCTCTGTG
RAD51-Exon3_For	CCCCTGGAAAGGATAATGAGA
RAD51-Exon4_For	AGGGATACAGTCTGCGGTTG
RAD51-Exon4_For	GGTCCTACCTTGCAGCAGTC
RAD51-Exon5_For	CATCTTTCTGATGAGCTCCAAG
RAD51-Exon5_For	TCCTAACAGATGCTTGCAAATAG
RAD51-Exon6_For	AAGATGTCATGAGGAGCTTGG
RAD51-Exon6_For	ACTTTGGGACGTGGGGTTA
RAD51-Exon7_For	TCAGTACCACTTCTTCCCTACC
RAD51-Exon7_For	AAACCTCCTCATTTCTAATTCAAAC
RAD51-Exon8_For	TTTTAGGGTGGTAAGGAAGGG
RAD51-Exon8_For	GGCGATGATATTTCCTCCAA
RAD51-Exon9_For	GCCTTGCTAGGAGGCTAAGA
RAD51-Exon9_For	GCATGTTAATTAGATTAGCAAGAGTTC
RAD51-Exon10_For	ATTCTGCCAGGTTGGAAATG
RAD51-Exon10_For	TTTCCCGGAAGCTTTATCCT
Primers for splicing analysis (PCR)	
RAD51-cDNA7_For	AGACCCAGCTCCTTTATCAAG
RAD51-cDNA10_Rev	CCTCTTCCTTTCCTCAGATACAA
Primers for AS RT-qPCR/ddPCR (PCR)	
GAPDH_For	AATCCCATCACCATCTTCCA
GAPDH_Rev	TGGACTCCACGACGTACTCA
RAD51-A-wt_For	AGGTTTCTGCGGATGCTTCTGC
RAD51-A-mut_For	AGGTTTCTGCGGATGCTTCTAT
RAD51-A_Rev	CACTTGAGCTACCACCTGATTAGTGA
RAD51-B-wt_For	GCAAAATCTACGACTCTCCCTG
RAD51-B-mut_For	GCAAAATCTACGACTCTCCGTC
RAD51-B_Rev	TTTCCCGGAAGCTTTATCCT
RAD51-C-wt_For	ATGATGGTAGAATCTAGGTA
RAD51-C-wt_Rev	CCACTTGAGCTACCACCTGA
RAD51-C-mut_For	GCCATGATGGTAGAATCTAGTTT
RAD51-C-mut_Rev	GGCGATGATATTTCCTCCAA
RAD51-D-wt_For	CCAGACCCAGCTCCTTTATC
RAD51-D-wt_Rev	TGATTACCACTGCTACACCAAA
RAD51-D-mut_For	CACCAGACCCAGCTCCTTTA
RAD51-D-mut_Rev	TCAGATACAATCTCATCAGCGAGT
RAD51-E-wt_For	CGTTCAACACAGACCACCAG
RAD51-E-mut_For	CTTGGCCAGGTTTCTGGA
RAD51-E_Rev	AGCGAGTCACAGAAGCATCC
RAD51-F-wt_For	GCTAAATTAGTTCCAATGGGTTTCACC
RAD51-F-mut_For	GCTAAATTAGTTCCAATGGGTTTCAGA
RAD51-F_Rev	GCTCTTTGGAGCCAGTAGTAATCTGT

Primers for minigene splicing assays (PCR for constructs and analysis)	
RAD51-B-Bam9_For	AAGAAGTGCAGGATCCAGGCTAAGACATCAGTGCC
RAD51-B-Mlu9_Rev	TCAAAACAAGACGCGTAACGAGAGCATGTTAATTAGATTAG
RAD51hs-896-1_For	GATCCCATCAACACCTTATCTGGTTGTTGATGCATGG
RAD51hs-896-1_Rev	CCATGCATCAACAACCAGATAAGGTGTTGATGGGATC
RAD51-D-Bam8_For	AAGAAGTGCAGGATCCCAGAGCTAGACTCCATCTCAAAAA
RAD51-D-Mlu8_Rev	TCAAAACAAGACGCGTTCTCTTCTTCCTAAGAGCTTGATG
pCAS-Seq_For	GGGGTCAATAGCAGTGAGAGG
pCAS-Seq_Rev	GCTCCATTTCACAGGTAGAGA
pCAS-KOI-F	TGACGTCGCCGCCCATCAC
pCAS-2R	ATTGGTTGTTGAGTTGGTTGTC
Primers for site-directed mutagenesis in RAD51-myc constructs	
RAD51-A89E_For	GCCTTTGGTGGAATTCAGTCTCAGTGGTGAAACCCATTGG
RAD51-A89E_Rev	CCAATGGGTTTCACCACTGAGACTGAATTCCACCAAAGGC
RAD51-A89T90del_For	TAGTTCCAATGGGTTTCACAACTGAATTCCACCAAAGG
RAD51-A89T90del_Rev	CCTTTGGTGGAATTCAGTTGTGAAACCCATTGGAACTA
RAD51-R250A_For	CGAGTCGCAGAAGCATGGCCAGAAACCTGGCCAAG
RAD51-R250A_Rev	CTTGGCCAGGTTTCTGGCCATGCTTCTGCGACTCG
RAD51-R250Q_For	GTCGCAGAAGCATCTGCAGAAACCTGGCC
RAD51-R250Q_Rev	GGCCAGGTTTCTGCAGATGCTTCTGCGAC
RAD51-T134N_For	GTATGACAGATCTGGTTCTTCCCAGTTCGGAATTC
RAD51-T134N_Rev	GAATTCCGAACTGGGAAGAACCAGATCTGTCATAC
Primers for cloning of EGFP-myc construct (PCR)	
EGFP_For	GGCCGGGAATTCGTCGACTGATGGTGAGCAAGGGCGAG
EGFP_Rev	AGATGAGTTTCTGCTCGAGCCTTGTACAGCTCGTCCATGC
Primers for cloning of RAD51-HA constructs (PCR)	
RAD51-HA_For	CCGGACTCAGATCTCGAGCTCATGGCAATGCAGATGCAG
RAD51-HA_Rev	GGAACATCGTATGGGTATGCGTCTTTGGCATCTCCCAC

Table S3. List of the antibodies used in this study.

Antibodies	Dilution	Used for	Identifier
Rabbit monoclonal anti-human RAD51	1/1,000	WB	Cat# 8875; RRID: AB_2721109
Rabbit polyclonal anti-human RAD51		IP	Cat# PC130; RRID: AB_2238184
Mouse monoclonal anti-human α-Tubulin	1/4,000	WB	Cat# T5168; RRID: AB_477579
Mouse monoclonal anti-human c-Myc	1/200	WB	Cat# sc-40; RRID: AB_627268
Sheep polyclonal anti-mouse IgG (H + L) HRP conjugated	1/10,000	WB	Cat# NXA931; RRID: AB_772209
Donkey polyclonal anti-rabbit IgG (H+L) HRP conjugated	1/10,000	WB	Cat# 711-036-152; RRID: AB_2340590

WB: western blot; IP: immunoprecipitation

References

1. Martinez JS, von Nicolai C, Kim T, et al. BRCA2 regulates DMC1-mediated recombination through the BRC repeats. *Proc Natl Acad Sci U S A* 2016;**113**:3515–20.
2. Woods BT, Teuber HL. Mirror movements after childhood hemiparesis. *Neurology* 1978;28(11):1152–7.
3. Depienne C, Bouteiller D, Méneret A, et al. RAD51 Haploinsufficiency Causes Congenital Mirror Movements in Humans. *Am J Hum Genet* 2012;90(2):301–7.
4. Franz EA, Chiaroni-Clarke R, Woodrow S, et al. Congenital mirror movements: Phenotypes associated with DCC and RAD51 mutations. *J Neurol Sci* 2015;351(1–2):140–5.